

# STREAMLINING THE DESIGN SPACE OF LEARNING AND SEARCH SUGGESTS DESIRABLE PRINCIPLES IN ML4TSP AND BEYOND

**Anonymous authors**

Paper under double-blind review

## ABSTRACT

Despite the rich works on machine learning (ML) for combinatorial optimization (CO), a unified, principled framework remains lacking. This study utilizes the Travelling Salesman Problem (TSP) as a major case study, with adaptations demonstrated for other CO problems, dissecting established mainstream learning-based solvers to outline a comprehensive design space. It advances a unified modular streamline incorporating existing technologies in both learning and search for transparent ablation, aiming to reassess the role of learning and to discern which parts of existing techniques are genuinely beneficial and which are not. This further leads to the investigation of desirable principles of learning designs and the exploration of concepts guiding method designs. We demonstrate the desirability of principles such as joint probability estimation, symmetry solution representation, and online optimization for learning-based designs. Leveraging the findings, we propose enhancements to existing methods to compensate for their missing attributes, thereby advancing performance and enriching the technique library. From a higher viewpoint, we also uncover a performance advantage in non-autoregressive and supervised paradigms compared to their counterparts. The strategic decoupling and organic recompositions yield a factory of new TSP solvers, where we investigate synergies across various method combinations and pinpoint the optimal design choices to create more powerful ML4TSP solvers, thereby facilitating and offering a reference for future research and engineering endeavors.

## 1 INTRODUCTION

Combinatorial Optimization (CO) has been a central challenge with its inherent complexity (e.g., NP-hardness). Recently, machine learning (ML) has been actively introduced to address CO problems, i.e., ML4CO (Bengio et al., 2021; Cappart et al., 2021), which brings practical advantages in both solving quality and speed especially when the instances are confined within a certain distribution (Bengio et al., 2021). Among CO problems, the Travelling Salesman Problem (TSP) has been representative as one of the most intensely studied problems in both ML4CO and Operations Research (OR) communities with one of the richest libraries of learning and search techniques (Hottung et al., 2021b; Fu et al., 2021; Min et al., 2023; Qiu et al., 2022; Hudson et al., 2021; Sun & Yang, 2023; Li et al., 2023; Kool et al., 2018; Kwon et al., 2020; Kim et al., 2022). For solving CO problems, deep neural networks enjoy high parallel computing ability for speedup through one-shot inference. Meanwhile, ML could automatically uncover heuristics through data (Kool et al., 2018; Luo et al., 2023) for improvement against existing handcrafted rules, especially for some new problems or new instance distributions that call for experts to develop tailored solving schemes.

Recent advancements in learning-based solvers have significantly enhanced their solving performance and capacity to tackle larger-scale problems. These improvements have been propelled by a variety of learning paradigms, encompassing supervised predictive modeling (Hottung et al., 2021b; Fu et al., 2021; Hudson et al., 2021), reinforcement learning (Qiu et al., 2022; Kool et al., 2018; Kwon et al., 2020; Kim et al., 2022), generative modeling (Sun & Yang, 2023; Li et al., 2023), unsupervised learning (Min et al., 2023), meta learning (Qiu et al., 2022), etc. In modern approaches, learning and search elements are often interleaved with each other, and common designs among existing learning-based solvers may manifest in varying implementations, making their effects and contributions less

054  
055  
056  
057  
058  
059  
060  
061  
062  
063  
064  
065  
066  
067  
068  
069  
070  
071  
072  
073  
074  
075  
076  
077  
078  
079  
080  
081  
082  
083  
084  
085  
086  
087  
088  
089  
090  
091  
092  
093  
094  
095  
096  
097  
098  
099  
100  
101  
102  
103  
104  
105  
106  
107

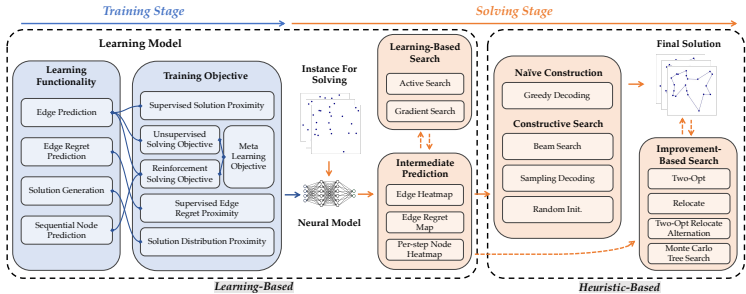


Figure 1: Overview of our proposed ML4TSP framework. Blue and orange stand for training and testing processes, respectively. Dashed lines indicate the optional processes in pipelines.

transparent, let alone their intricate interplay. Meanwhile, the lack of crisp analysis of the whole ML4TSP system (a representative example for ML4CO) hinders the determination of the role of learning and the establishment of desirable principles for learning designs.

In this paper, we adopt a higher-level perspective to consider the whole system and advocate the necessity of inspecting and aligning various existing methods. We endeavor to decompose established mainstream learning-based solvers to outline a comprehensive design space and unify a modular streamline incorporating aligned learning and search technologies while minimizing disparities among methods, facilitating transparent ablation and systematic analysis. Fig. 1 presents the overview of our framework. Given instances and their (optional) labels e.g. reference solutions, the training stage involves different learning functionalities and training objectives to exploit the effective heuristics from data. Given instances, the solving stage follows a construction-refinement pipeline whereby a complete (feasible) solution is generated first then it is improved through the improvement-based search. The construction is based on the intermediate predictions produced by the trained model, and learning-based search is optionally applied to improve prediction quality by updating the parameters of the model or the intermediate predictions. Note the prediction results for auto-regressive methods using sequence models (Kool et al., 2018; Kwon et al., 2020) involve the interplay of neural models and construction methods to update the node heatmap prediction for different steps.

Based on this framework, we analyze the correlation between learning and solving objectives along with the efficacy of current ML4TSP endeavors within the outlined framework. This further leads to the summarization of the inherent desirable design principles among diverse learning methods and discerns key attributes that contribute to performance improvement. Specifically, minimized ablation studies are performed demonstrating the desirability of design principles such as joint probability estimation, symmetry solution representation, online optimization, and search friendliness. Additionally, we offer insights into how model predictions intervene with strong search methods like MCTS and highlight preferences in learning paradigms (e.g., supervised vs. unsupervised, autoregressive vs. nonautoregressive) regarding solving performance and scalability.

Leveraging our findings, we propose enhancements to existing methods to compensate for their missing attributes, thereby advancing performance and enriching the technique library. Examples of novel methods include node-level normalization for one-shot solution predictions (Joshi et al., 2019), symmetry introduction into the diffusion-based solvers (Sun & Yang, 2023; Li et al., 2023) and the reinforcement solving objective of Qiu et al. (2022), the devised MCTS variants by decoupling the dependencies between solution initialization and local search within MCTS (Fu et al., 2021) and connecting its local search component with established constructive search methods, etc. Furthermore, we re-compose within the established technique library and propose a factory of solvers, among which the optimal ones achieve performance gains over previous SOTA. Beyond TSP, we also demonstrate adaptations of the framework to other CO problems and verify that the desirability of design principles discovered in ML4TSP evaluations still holds for other CO problems. Our implementation is carefully organized, featuring solver classes for various learning functionalities, facilitating easy development for further research and engineering practices. We aim for this work to streamline the development and evaluation process, offering a consistent implementation for verifying the effects of proposed methods efficiently.

## 2 PRELIMINARIES AND RELATED WORK

**Graph Combinatorial Optimization and Travelling Salesman Problem (TSP).** Following Karalias & Loukas (2020); Wang et al. (2022), we define  $\mathcal{G}$  as the universe of CO instances by graphs

$G(V, E) \in \mathcal{G}$ , where  $V$  and  $E$  denote the node set and edge set respectively. Let  $\mathbf{x} \in \{0, 1\}^N$  denote the optimization variable and  $\Omega$  denotes the feasible set. A CO problem on  $G$  aims to find a feasible  $\mathbf{x} \in \Omega$  that minimize the given objective function  $f(\cdot; G) : \Omega \rightarrow \mathbb{R}_{\geq 0}$ . TSP is defined on an undirected complete graph  $G = (V, E)$ , where  $V$  represents  $n$  cities and each edge  $E_{i,j}$  has a non-negative weight  $\mathbf{D}_{i,j}$  representing the distance between cities  $i$  and  $j$ . The problem is to find a Hamiltonian cycle of minimum weight in  $G$ . Here the dimension of the optimization variable  $N = n^2$ , and we denote the solution as a matrix  $\mathbf{X} \in \{0, 1\}^{n \times n}$  where  $\mathbf{X}_{i,j}$  indicates whether  $E_{i,j}$  is included in  $\mathbf{x}$ . The objective function is:  $f(\mathbf{X}; G) = \mathbf{D} \odot \mathbf{X} = \sum_{i,j} \mathbf{D}_{i,j} \cdot \mathbf{X}_{i,j}$ .

**Related Works.** Learning-based designs have advanced CO (Bengio et al., 2021; Cappart et al., 2021; Peng et al., 2021). TSP has long been studied by the machine learning community since early works like (Vinyals et al., 2015; Khalil et al., 2017; Nowak et al., 2017) and is one of the most extensively studied CO problems. Other CO problems like MIS (Brusca et al., 2023; Goshvadi et al., 2024; Wang & Li, 2023), CVRP (Ma et al., 2024; Hou et al., 2023; Kim et al., 2023) are also widely studied, which can sometimes share similar methodology designs. To our knowledge, this is the first endeavor to rethink the existing system and methodologies in ML4TSP while concurrently pioneering the development of new effective techniques. This stands in contrast to Berto et al. (2023) which primarily focused on providing a unified implementation and evaluation of RL-based models without delving into deeper analyses of learning paradigms and proposing new methods. Joshi et al. (2020) tries to analyze from the generalization perspective, yet the investigated methods are confined to naive pipelines (Kool et al., 2018; Joshi et al., 2019) which is a very partial subset of the current ML4TSP system, and no general design principles or new methods are provided as well. Our framework tries to integrate every mainstream effort of constructive ML4TSP solvers. The comprehensive nature of our framework facilitates a higher-level integration and analysis of the ML4TSP system, thereby facilitating the development of a broader spectrum of research avenues within the community.

### 3 MODULAR FRAMEWORK FOR ML4TSP SOLVERS

#### 3.1 DESIGN SPACE FOR TRAINING STAGE ALGORITHMS

The learning models generally receive input features from the instance graph, where the typical features optionally include node features indicating the 2D coordinates of the nodes, and edge features indicating the weight of the edges. The network backbones include GNN variants like Graph Convolutional Networks (GCN) (Kipf & Welling, 2016; Joshi et al., 2019), Graph Attention Networks (GAT) (Veličković et al., 2017; Kool et al., 2018), and Scattering Attention GNN (SAG) (Min et al., 2023). The algorithmic variances are reflected in the learning functionalities and training objectives presented below, where the correlations between these components are presented in Fig. 1.

##### 3.1.1 LEARNING FUNCTIONALITIES

Different learning functionalities are proposed to more efficiently utilize data for solving TSP, which involves what the neural models learn from pre-existing data.

**Edge Prediction.** Joshi et al. (2019); Fu et al. (2021); Qiu et al. (2022); Min et al. (2023) frame TSP solving as an edge prediction task, where each edge is classified as binary to determine whether it is in the solution. The prediction confidence of the edges (after softmax function) serves as a heatmap  $\mathbf{H}$  denoting the probabilities of edges occurring in the tour, i.e.,  $\mathbf{H}_{i,j} = p(E_{i,j} \in \mathbf{S}^*)$  where  $\mathbf{S}^*$  denotes the optimal solution represented in the matrix form.

**Edge Regret Prediction.** The global regret is defined as the cost of fixing a certain edge in the solution relative to the cost of a globally optimal solution (Hudson et al., 2022):  $\mathbf{R}_{i,j} = \frac{f(\mathbf{S}_{i,j}^*; G)}{f(\mathbf{S}^*; G)} - 1$  where  $\mathbf{R}_{i,j}$  denotes the regret of selecting  $E_{i,j}$  in the solution,  $\mathbf{S}_{i,j}^*$  denotes the optimal solution with  $E_{i,j}$  fixed, and  $\mathbf{S}^*$  is the global optimal solution. This target contains more knowledge about how every edge benefits the optimization, especially for edges not included in the optimal solution, making it more conducive to searching. However, it necessitates significantly more computational resources to acquire the supervision.

**Solution Generation.** Deviating from the prediction of a single solution, generative modeling methods (Sun & Yang, 2023; Li et al., 2023; Hottung et al., 2021a) endeavor to characterize a distribution of high-quality solutions for a given instance, i.e., estimating  $p(\mathbf{S}|G)$ . Solutions can be

established by sampling from the distribution. This consideration of distributions makes predictions more diverse, thereby enhancing the search.

**Sequential Node Prediction.** Instead of global prediction in one shot, sequence models (Kool et al., 2018; Kwon et al., 2020; Kim et al., 2022) decompose it into  $n$ -step node predictions, where each step offers the prediction map of the next node selection based on the current state. The sequence models generally follow an attention based encoder-decoder model where the encoder produces embeddings of all input nodes and the decoder produces the per-step node heatmap predictions  $\mathbf{h}_j^{(i)} = p(\pi_i = j | \pi_{<i})$  where  $\mathbf{h}_j^{(i)}$  is the  $j$ -th element of step  $i$ 's prediction map and  $\pi$  is the permutation representation of the solution.

### 3.1.2 TRAINING OBJECTIVES

Training objectives are proposed to achieve the learning functionalities in Sec. 3.1.1. This subsection discusses supervised and unsupervised methods sequentially. Supervised methods effectively leverage the readily available solved data, while unsupervised methods bypass the need to acquire supervision.

**Supervised Solution Proximity.** This objective encourages the model's prediction, e.g. heatmap  $\hat{\mathbf{H}} \in [0, 1]^{n \times n}$ , to approximate the reference solutions obtained by an alternative solver. Based on the binary classification for edges, the (weighted) binary cross-entropy loss is widely adopted:

$$\mathcal{L} = - \sum_{i,j} w_1 \cdot \mathbf{S}_{i,j} \cdot \log(\hat{\mathbf{H}}_{i,j}) + w_0 \cdot (1 - \mathbf{S}_{i,j}) \cdot \log(1 - \hat{\mathbf{H}}_{i,j}) \quad (1)$$

where  $w_0, w_1$  are class weights since the classification task is unbalanced towards the negative class.

**Supervised Edge Regret Proximity.** This objective encourages the model to predict reliable edge regrets  $\hat{\mathbf{R}} \in \mathbb{R}^{n \times n}$  to approximate the reference regrets  $\mathbf{R}$ , by minimizing  $\mathcal{L} = \|\hat{\mathbf{R}} - \mathbf{R}\|_2$ .

**Solution Distribution Proximity.** Prominent models for the generative objective encompass diffusion models (Sun & Yang, 2023; Li et al., 2023) and variational autoencoders (VAE) (Hottung et al., 2021a), to maximize the conditional likelihood estimation  $\mathbb{E}[\log p_\theta(\mathbf{S}|G)]$ , where  $\theta$  is the model parameters. The models are typically optimized through the evidence lower bound (ELBO), where  $q$  is the posterior and  $\mathbf{Z}$  is the latent variable.

$$\mathcal{L} = -\mathbb{E}_{q(\mathbf{Z}|\mathbf{S}, G)} \left[ \log \frac{p_\theta(\mathbf{S}, \mathbf{Z}|G)}{q(\mathbf{Z}|\mathbf{S}, G)} \right] \geq \mathbb{E}[-\log p_\theta(\mathbf{S}|G)] \quad (2)$$

Unsupervised methods typically optimize using the solving objective. However, the non-differentiable mapping from continuous, unconstrained space to discrete, highly constrained space suffers gradient truncation. Thus, unsupervised loss based on constraint penalty and reinforcement solving loss are employed, and meta-learning can be further adapted to enhance generalization.

**Unsupervised Solving Objective.** Min et al. (2023) proposes penalties over the Hamiltonian cycle and no self-loop constraints to regularize the predicted assignment matrix  $\hat{\mathbf{T}}$  and heatmap  $\hat{\mathbf{H}}$ .  $\hat{\mathbf{T}}$  is obtained by enforcing column-wise softmax to the network output, where  $\hat{\mathbf{T}}_{\cdot,j} \in [0, 1]^{n \times 1}$  indicates the next-node probabilities at  $i$  step, and  $\hat{\mathbf{H}}$  is calculated through  $\hat{\mathbf{H}} = \hat{\mathbf{T}}_{\cdot,n} \hat{\mathbf{T}}_{\cdot,1}^\top + \sum_{t=1}^n \hat{\mathbf{T}}_{\cdot,t} \hat{\mathbf{T}}_{\cdot,t+1}^\top$ :

$$\mathcal{L} = \sum_{i,j} \hat{\mathbf{H}}_{i,j} \mathbf{D}_{i,j} + \lambda_1 \sum_i \left( \sum_j \hat{\mathbf{T}}_{i,j} - 1 \right)^2 + \lambda_2 \sum_i \hat{\mathbf{H}}_{i,i}. \quad (3)$$

The second and third term denotes the Hamilton cycle and no self-loop constraint, respectively.

**Reinforcement Solving Objective.** With the predicted probability distribution  $p_\theta(\mathbf{S}|G)$ , we can sample solution tours. This objective optimizes the expectation of the tour length by gradient estimated by REINFORCE (Williams, 1992) with baseline  $b(G)$ :

$$\mathcal{L} = \mathbb{E}_{p_\theta(\mathbf{S}|G)} [f(\mathbf{S}; G)] \quad \text{and} \quad \nabla \mathcal{L} = \mathbb{E}_{p_\theta(\mathbf{S}|G)} [(f(\mathbf{S}; G) - b(G)) \nabla \log p_\theta(\mathbf{S}|G)] \quad (4)$$

where the baseline function independently estimates the expected cost to reduce the variance of the gradients. The sampling construction method presented in Sec. 3.2.2 enables sampling solutions from the predicted edge heatmap and per-step node heatmaps to achieve  $p_\theta(\mathbf{S}|G)$ .

**Meta-Learning Objective.** This objective (Finn et al., 2017; Qiu et al., 2022) aims to train models to acquire meta-knowledge from diverse problem instances, improving generalization when faced with

216 previously unseen instances. In CO, model parameters and model predictions can be further updated  
 217 during testing through a learning-based search in Sec. 3.2.1. The objective tries to better predict a  
 218 model initialization or prediction that can achieve the best solving results after the learning-based  
 219 search in the solving phase. Suppose the edge heatmap  $\hat{\mathbf{H}}$  is optimized to  $\hat{\mathbf{H}}'$ , then the meta-learning  
 220 objective is  $\mathcal{L} = \mathbb{E}_{p_s(\mathbf{S}|G, \hat{\mathbf{H}}')} [f(\mathbf{S}; G)]$  where  $s(\cdot)$  denotes the sampling decoding function.  
 221

## 222 3.2 DESIGN SPACE FOR SOLVING STAGE ALGORITHMS

223 The solving stage does not involve any pre-existing data but tries to optimize the solutions or the  
 224 predictions over unseen instances received on the fly, as shown in Fig. 1.  
 225

### 226 3.2.1 LEARNING-BASED SEARCH

227 Motivated by the divergence between the training stage, which optimizes average performance across  
 228 historical instances, and the solving stage, which optimizes performance for each new instance,  
 229 Hottung et al. (2021b); Qiu et al. (2022); Li et al. (2023) design learning-based search in the solving  
 230 stage to perform tailored optimization for testing instances, which improves prediction by updating  
 231 the model parameters or the intermediate predictions.  
 232

233 **Active Search.** With objectives that do not require labels, active search (Hottung et al., 2021b; Qiu  
 234 et al., 2022) further fine-tunes (partial) network parameters or intermediate model predictions, e.g.  
 235 heatmaps, over each testing instance with solving objective updates of Eq. 4 using gradient decent.

236 **Gradient Search.** Based on diffusion modeling (Sun & Yang, 2023), T2T (Li et al., 2023) introduces  
 237 objective guidance into the denoising process of diffusion, adjusting the denoising to an objective-  
 238 minimizing direction and rewriting the original learned denoising function  $p_\theta(\mathbf{S}_{t-1}|\mathbf{S}_t, G)$  to

$$239 p_\theta(\mathbf{S}_{t-1}|\mathbf{S}_t, G, y^*) = Z p_\theta(\mathbf{S}_{t-1}|\mathbf{S}_t, G) \exp([- \nabla_{\mathbf{S}_t} \tilde{l}(\mathbf{S}_t; G)]^\top \mathbf{S}_{t-1}) \quad (5)$$

240 where  $y^*$  is the optimal objective score given the instance  $G$ ,  $\tilde{l}$  denotes the objective estimation  
 241 function. This technique allows for further refinement of the predicted heatmaps by iteratively adding  
 242 noise to the current solution and then denoising it to an expected better one.  
 243

### 244 3.2.2 CONSTRUCTION METHODS

245 Construction methods typically leverage the predictions and the graphs to decode a complete solution.

246 **Greedy Decoding.** As a naive construction method, it sequentially inserts edges/nodes with the  
 247 highest confidence in the heatmap to the partial solution for a feasible solution.  
 248

249 **Sampling Decoding.** It involves sampling edges or nodes based on their confidence scores in the  
 250 heatmaps. Denoting  $\pi$  as the permutation representation of  $\mathbf{S}$ , based on the edge heatmap  $\hat{\mathbf{H}}$ , the  $t$ -step  
 251 node heatmap prediction can also be estimated from the edge heatmap  $\hat{\mathbf{h}}^{(t)} = \frac{\exp(\hat{\mathbf{H}}_{\pi_{t-1}, \pi_t})}{\sum_{j=i}^n \exp(\hat{\mathbf{H}}_{\pi_{t-1}, \pi_t})}$ .  
 252

253 **Beam Search.** At each step, beam search (Joshi et al., 2019) explores the heatmap by expanding the  $b$   
 254 most probable edge connections among the nodes neighbors and saving the best  $b$  partial solutions for  
 255 the next step. The final prediction is the tour with the highest probability among the  $b$  complete tours.  
 256

257 **Random Initialization.** For strong improvement-based search methods like MCTS, random initial-  
 258 ization of tours can also produce plausible results.

### 259 3.2.3 IMPROVEMENT-BASED SEARCH

260 On top of the constructed complete solutions, improvement-based search further iteratively refines  
 261 solutions by exploring within a limited neighborhood of the current solution.  
 262

263 **Two-Opt and Relocate.** Two-Opt swaps two nodes in the tour, dividing it into three segments, then  
 264 reassembles the tour by reversing the middle segment. The relocate operator moves a single node  
 265 within the tour. The operators can be performed on the original solution to find lower-cost ones. These  
 266 two operators can be combined by alternating between using either operator until no better solution  
 267 can be found, which we call local search (LS) following Hudson et al. (2021) in the rest of the paper.

268 **Monte Carlo Tree Search.** The MCTS solver (Fu et al., 2021) iteratively proposes initial solutions  
 269 and improves them to enhance solution quality. In each iteration, this process includes three compo-  
 nents: 1) state initialization constructs a solution based on a given heatmap; 2) Two-Opt improvement

explores a small neighborhood by Two-Opt until no improvements can be found; 3) MCTS based on K-Opt iteratively samples K-Opt operators based on the heatmap to improve the solution and update the heatmap for subsequent iterations. Typically, thousands of iterations of these steps are involved in an MCTS solver. However, we observed that increasing the number of outer iterations results in diminishing marginal improvements in heatmap updating. Thus, we reduce the number of outer iterations to one round, separating the construction phase and the improvement-based search phase. We adopt the latter as a design choice for improvement-based search, which can be integrated with construction methods such as greedy, sampling, beam search, and random initialization to generate MCTS variants.

**Prediction Guidance.** Improvement-based search can be guided by edge regret prediction (Hudson et al., 2021), where the edge scores for penalizing is calculated as  $\frac{\hat{R}_{i,j}}{1+n_{i,j}}$ , where  $n_{i,j}$  is the number of penalties assigned to  $E_{i,j}$ . The edges of maximum utility are penalized and the search is applied only to the penalized edge to maximize the chance of finding lower-cost solutions.

## 4 EMPIRICAL EVALUATION

This section tries to answer the following questions and proposes new techniques: **Q1.** *How does learning benefit testing stage problem solving?* **Q2.** *What are the desirable design principles for ML4TSP methods?* **Q3.** *Which combination can enhance solving performance?* The major empirical evaluation is conducted on TSP, yet Appendix B also shows examples of adapting the ML4TSP framework to other problems like Capacitated Vehicle Routing Problem (CVRP) and Maximum Independent Set (MIS) and verify whether conclusions drawn from TSP still hold for other problems.

### 4.1 EXPERIMENTAL SETUP

**Datasets.** A TSP instance includes  $N$  2-D coordinates and a reference solution. Instances are generated via uniformly sampling  $N$  nodes from the unit square  $[0, 1]^2$ . Main experiments are performed on TSP on scales including 50, 100, and 500. We also include TSP-1000 and the real-world TSPLIB<sup>1</sup> dataset for generalization evaluation. The reference solutions for all problem scales are labeled by LKH-3 (Helsgaun, 2017). The test set for TSP-50/100 is taken from Kool et al. (2018) with 1,280 instances, and the test set for TSP-500/1000 is from Fu et al. (2021) with 128 instances.

**Metrics.** 1) Drop: the relative performance drop w.r.t. length compared to the optimal solutions (obtained by the exact solver Concorde (Applegate et al., 2006) in this paper); 2) Time: the average computational time per instance; 3) Length: the average total distance of the solved tours w.r.t. the corresponding instances i.e. the objective. Note the main paper omits this metric and indicates solution quality primarily by drop for clearness. Full results are presented in Appendix Table 9.

**Method Indicator.** We explore various combinations within the design space depicted in Fig. 1, making it impractical to label each variant individually. Thus, we directly list the design choices of the evaluated methods in the tables as indicators. Note the ablation may lead to convergence towards a subset of methods with common designs. In such cases, shared design choices are omitted from the table and explained in the caption for clarity. **To correspond to prior methods, please refer to Table 9.** To simplify method indication in experiments, we adopt the following abbreviations for certain design choices in our ML4TSP framework: 1) Learning Functionalities: Edge Prediction → Edge Pred, Edge Regret Prediction → Regret Pred, Solution Generation → Generation, Sequential Node Prediction → Sequential; 2) Training Objectives: Supervised Solution Proximity → SL, Supervised Edge Regret Proximity → SL Regret, Unsupervised Solving Objective → UL, Reinforcement Solving Objective → RL, Solution Distribution Proximity → Generative.

### 4.2 LEARNING GENERALLY IMPROVES SOLVING WITH COMPATIBLE SEARCH ALGORITHMS

This subsection endeavors to answer **Q1**. Apart from the training objectives that optimize the solving performance, the reference proximity objectives are not directly related to the solving target. Since the solving performance relies on the synergy of neural predictions and search strategies, the correlation between the estimation accuracy in training and the final solving performance remains unclear. To verify this, Fig. 2 provides the scatter plots for the correlation between solving performance and the learning loss across reference proximity objectives on TSP-100 test sets.

<sup>1</sup><http://comopt.ifi.uni-heidelberg.de/software/TSPLIB95/>

Table 1: Joint probability estimation ablation based on methods with *Edge Pred* as the learning functionality.  $8 \times$  Greedy: sample 8 heatmaps in parallel then enforce greedy.

Objective	Joint Prob.	Solving Stage		TSP-50		TSP-100		TSP-500	
		Construction	Impr. Search	Drop↓	Time	Drop↓	Time	Drop↓	Time
SL	✗	Greedy	–	1.530%	7.6ms	7.078%	10.6ms	12.237%	0.1s
SL + Node Norm	✓	Greedy	–	0.674%	7.4ms	2.721%	10.1ms	8.496%	0.1s
Generative	✓	Greedy	–	<b>0.076%</b>	0.229s	<b>0.186%</b>	0.4s	<b>6.734%</b>	1.6s
SL	✗	Greedy	2-Opt	0.115%	7.6ms	0.649%	12.0ms	2.089%	0.1s
SL + Node Norm	✓	Greedy	2-Opt	0.082%	7.4ms	0.292%	11.7ms	1.325%	0.1s
Generative	✓	Greedy	2-Opt	<b>0.046%</b>	0.2s	<b>0.077%</b>	0.4s	<b>0.811%</b>	1.6s
SL	✗	Beam (n=1280)	–	0.023%	1.1s	0.673%	2.3s	23.629%	11.6s
SL + Node Norm	✓	Beam (n=1280)	–	0.016%	1.1s	0.545%	2.2s	21.678%	13.7s
Generative	✓	$8 \times$ Greedy	–	<b>0.007%</b>	0.7s	<b>0.011%</b>	2.5s	<b>1.476%</b>	10.3s
SL	✗	Beam (n=1280)	2-Opt	0.015%	1.1s	0.149%	2.3s	2.431%	12.9s
SL + Node Norm	✓	Beam (n=1280)	2-Opt	0.012%	1.1s	0.156%	2.3s	2.189%	14.0s
Generative	✓	$8 \times$ Greedy	2-Opt	<b>0.006%</b>	0.7s	<b>0.009%</b>	2.5s	<b>0.303%</b>	10.4s

Overall, there exists a positive correlation between learning quality and problem-solving performance. However, the introduction of a more robust search mechanism tends to mitigate the advantages of neural predictions. Moreover, once the learning loss surpasses a certain threshold (e.g., less than 0.003 for the distribution objective), the efficacy of translating improvements in neural predictions into enhancements in problem-solving quality may diminish. This suggests a potential bottleneck in the capacity of the learning phase to enhance the testing phase. Regarding the prediction of edge regret, we find that the accuracy of regret estimation minimally impacts improvement-based search methods without heatmap guidance, such as Two-Opt. More results of the effects of learning to MCTS are presented in Appendix D.8.

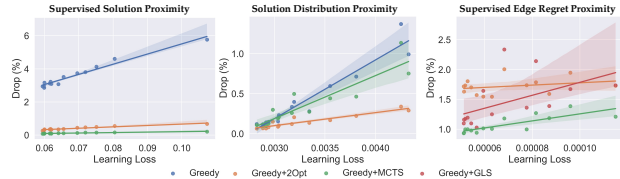


Figure 2: Performance correlation of three reference proximity objectives. GLS: guided local search.

4.3 DESIRABLE DESIGN PRINCIPLES THAT BENEFITS ML4TSP SOLVING

This subsection delves into crucial design principles in learning algorithms to answer Q2. We generalize overarching design principles with wide applicability across various learning designs, serving as foundational guidance that inspires methodological proposals. Building upon these principles, we introduce novel designs seamlessly integrated into existing pipelines to boost solving performance and validate the effectiveness of adhering to these principles throughout the process.

### 4.3.1 JOINT PROBABILITY ESTIMATION HELPS CAPTURE VARIABLE CORRELATIONS

This subsection validates the importance of joint probability estimation over solution variables in loss design. In the learning functionality of edge prediction, the *SL* training objective (Joshi et al., 2019; Fu et al., 2021) generally enforces supervision over each edge’s binary classification results. This is based on the assumption of mutual statistical independence of the individual solution parameters, such that the solution can be represented by a product of Bernoulli distributions for the individual solution variables Sanokowski et al. (2023). However, since the CO solutions are highly constrained with strong correlations among the solution variables, such an assumption can lead to a performance drop.

#### 4.3.1.1 JOINT PROBABILITY ESTIMATION HELPS CAPTURE VARIABLE CORRELATIONS

With GNN raw predictions  $\mathbf{F} \in \mathbb{R}^{n \times n \times 2}$ , which correspond to  $n \times n$  edges, prior methods utilize the softmax operation over the last dimension to ensure that the probabilities of positive and negative edges sum up to 1. The cross-entropy loss in Eq. 1 involves  $n \times n$  edges’ binary classification, lacking a general capture of joint probability over the solution variables. To this end, we propose node-wise probability normalization, which normalizes the positive edge probabilities associated with each node sum up to 2 and the negative probabilities sum to  $n - 2$ :  $\mathbf{F}'_{i,j} = \frac{\exp(\mathbf{F}_{i,j})}{\sum_{k=i}^n \exp(\mathbf{F}_{i,k})} \cdot \begin{bmatrix} n - 2 & 0 \\ 0 & 2 \end{bmatrix}$ .

Then it clips the probability to (0,1]. The predicted heatmap is obtained by  $\hat{\mathbf{H}} = \mathbf{F}'[:, :, 1]$ .

Under the edge prediction functionality, we also include methods of solution distribution proximity objective into comparison, which considers a solution as the whole entity, allowing it to naturally adhere to the joint probability distribution. Table 1 shows the ablation. Methods with joint probability

Table 2: Symmetry ablation based on methods with *Generative* as training objective.

Symmetry	Solving Stage		TSP-500	
	Construction	Impr. Search	Drop↓	Time
✗	Greedy	–	9.639%	1.2s
✓	Greedy	–	<b>6.734%</b>	1.6s
✗	Greedy	2-Opt	1.524%	1.2s
✓	Greedy	2-Opt	<b>0.811%</b>	1.6s
✗	8× Greedy	–	4.613%	6.9s
✓	8× Greedy	–	<b>1.476%</b>	10.3s
✗	8× Greedy	2-Opt	0.686%	6.9s
✓	8× Greedy	2-Opt	<b>0.303%</b>	10.4s

Table 3: Symmetry ablation based on methods with *RL* as the training objective. AS: active search.

Functionality	Symmetry	Solving	TSP-50		TSP-100	
			Drop↓	Time	Drop↓	Time
Edge Pred	✗	Sampling	5.238%	11.4ms	9.364%	94.5ms
+ Rand. Start	✓	Sampling	<b>2.157%</b>	72.7ms	<b>4.885%</b>	0.1s
Edge Pred	✗	AS+Sampling	3.086%	3.2s	4.234%	6.7s
+ Rand. Start	✓	AS+Sampling	<b>0.823%</b>	4.9s	<b>2.089%</b>	9.3s
Sequential	✗	Greedy	1.040%	0.1ms	2.520%	0.2ms
+ MultiStart	✓	Greedy	<b>0.179%</b>	1.7ms	<b>1.641%</b>	1.6ms
+ Sym. Baseline	✓	Greedy	0.877%	0.6ms	2.209%	0.6ms
Sequential	✗	Sampling	1.212%	0.1ms	2.846%	0.2ms
+ MultiStart	✓	Sampling	<b>0.156%</b>	1.3ms	<b>1.618%</b>	1.6ms
+ Sym. Baseline	✓	Sampling	1.041%	0.6ms	2.593%	0.6ms

Table 4: Ablation on online optimization property, which can be achieved by learning-based search.

Functionality	Objective	Solving Stage			TSP-50		TSP-100		TSP-500	
		Learning Search	Construction	Impr. Search	Drop↓	Time	Drop↓	Time	Drop↓	Time
Generation	Generative	✗	Greedy	–	0.076%	0.2s	0.186%	0.4s	6.734%	1.6s
	Generative	Gradient Search	Greedy	–	<b>0.015%</b>	0.7s	<b>0.023%</b>	0.8s	<b>2.666%</b>	3.7s
	Generative	✗	Greedy	2-Opt	0.046%	0.2s	0.077%	0.4s	0.811%	1.6s
	Generative	Gradient Search	Greedy	2-Opt	<b>0.012%</b>	0.7s	<b>0.023%</b>	0.8s	<b>0.442%</b>	3.8s
Edge Pred	Meta + RL	✗	Sampling	–	4.310%	35.9ms	4.885%	0.1s	13.046%	1.3s
	Meta + RL	Active Search	Sampling	–	<b>3.006%</b>	2.9s	<b>3.940%</b>	8.5s	<b>6.924%</b>	274.8s
	Meta + RL	✗	Sampling	2-Opt	1.821%	0.1s	2.880%	0.2s	6.228%	6.4s
	Meta + RL	Active Search	Sampling	2-Opt	<b>1.549%</b>	4.4s	<b>2.176%</b>	8.9s	<b>4.322%</b>	277.0s

estimation generally achieve lower drops, while relying solely on the proposed node-wise probability normalization can bring about significant performance improvement **without any additional computational overhead**. The generative objective can achieve much lower drops, albeit with the added computational cost of multistep inference in the diffusion model.

### 4.3.2 SYMMETRY SOLUTION REPRESENTATION INTRODUCES EQUIVALENCE AWARENESS

A tour solution holds symmetry or permutation invariance (Kwon et al., 2020). For instance, let tour  $\pi = \{v_1, v_2, v_3, v_4\}$  be the optimal solution of some given 4-node TSP instance. Then tours with different starting points, e.g.  $\pi' = \{v_2, v_3, v_4, v_1\}$ , and tours in a counterclockwise direction, e.g.  $\pi'' = \{v_4, v_3, v_2, v_1\}$ , all represent the same optimal solution. Since CO aims to produce optimal solutions, the neural model is expected to be aware of the equivalences among such sequences and should be optimized to consistently yield the same solution regardless of the variances in forms. This subsection endeavors to introduce the symmetry solution representation attribute to methods lacking symmetry consideration within the framework, thereby enhancing problem-solving performance.

For *Generation* learning functionality with *Generative* training objective, Sun & Yang (2023); Li et al. (2023) aim to generate directed graph representations (heatmaps) of solutions with directed graph supervision enforced in the optimization of Eq. 2. We replace the directed graph representation for learning with the undirected one, which naturally accommodates the symmetry, and discover a notable performance gain in Table 2. This does not explicitly increase computation during the learning process, but it introduces a slight overhead during solution decoding.

For the *RL* objective, methods decode solutions sequentially during optimization. For instance, Qiu et al. (2022) sequentially sample multiple solutions based on the predicted edge heatmap, all starting from the same point, to estimate the route length expectations and the REINFORCE gradients, and sequence models (Kool et al., 2018) predict node sequence using per-step node heatmaps for optimization. To achieve symmetry, we propose to enforce a random starting point decoding policy in REINFORCE updates (in training and active search) for methods with *Edge Pred* functionality, and refer to Kwon et al. (2020) to optimize over diverse rollouts with multiple starting points as well as use symmetry baselines (Kim et al., 2022) for *Sequential* functionality. These techniques raise the model’s awareness of symmetry. Table 3 presents solving results on TSP-50 and 100, showing a notable performance gain by introducing symmetry, yet with additional computational overhead.

### 4.3.3 ONLINE OPTIMIZATION COMPLEMENTS GENERALIZATION CAPABILITY

In order to bridge the gap between training for average performance and solving for performance in new instances, instance-specific optimization can be helpful. We verify the effectiveness of techniques that optimize in the testing phase in Sec. 3.2.1: the active search for methods with *Edge Pred* as the functionality and the gradient search for methods with *Generative* as the functionality. Table 4 ablates



Table 6: Heuristic search ablation based on *Edge Pred* functionality and *SL* training objective.

Solving Stage		TSP-50		TSP-100		TSP-500	
Construction	Impr. Search	Drop↓	Time	Drop↓	Time	Drop↓	Time
Greedy	–	1.530%	7.6ms	7.078%	10.6ms	12.237%	0.1s
Beam (n=1280)	–	0.023%	1.1s	0.673%	2.3s	23.629%	11.6s
MCTS Solver (10t)		0.006%	56.7ms	0.006%	0.217s	0.433%	10.1s
Greedy	Two-Opt	0.115%	7.6ms	0.649%	12.0ms	2.089%	0.1s
Greedy	Guided LS (t=1s)	0.614%	1.1s	3.319%	1.2s	7.682%	45.5s
Greedy	MCTS	0.018%	8.4ms	0.154%	16.8ms	0.838%	1.3s
Beam (n=1280)	Two-Opt	0.015%	1.1s	0.149%	2.3s	2.431%	12.9s
Beam (n=50)	MCTS	0.005%	0.1s	0.009%	0.5s	<b>0.235%</b>	56.3s
Sampling (n=50)	MCTS	0.002%	0.1s	0.001%	0.5s	0.396%	58.1s
Random (n=10)	MCTS	0.004%	17.5ms	0.011%	81.4ms	0.519%	11.2s
Random (n=50)	MCTS	<b>0.002%</b>	62.5ms	<b>0.001%</b>	0.4s	0.301%	55.2s

learning-based search across different baselines, indicating a promising gain with learning-based search, [however at the cost of additional computation](#).

#### 4.3.4 SEARCH FRIENDLINESS CONTRIBUTES TO LEARNING-SEARCH SYNERGY

Techniques that consider how to better integrate learning with search can benefit problem-solving. This subsection verifies the effectiveness of search friendliness designs including enhancing the informativeness of prediction information (e.g. predicting edge regrets), promoting diversity in the predicted solutions (e.g. modeling solution distribution), and incorporating the search process into optimization (e.g. through meta learning to learn optimal initialization for solving stage). Table 5 verifies the solving performance of providing more informative prediction and adopting meta learning, [which may also introduce slight overhead](#). We notice that for MCTS, the performance gain of predicting edge regrets is minor, which may stem from the compatibility between the techniques. For the effectiveness of prediction diversity, Table 2 demonstrates a significant improvement in solving performance achieved by employing multiple sampling, which is contributed by increased diversity.

Table 5: Ablation on search friendliness property.

Functionality	Objective	Search Frnd.	Solving Stage	TSP-50		TSP-100	
				Drop↓	Time	Drop↓	Time
Edge Pred	SL	✗	Guided LS (t=1s)	0.614%	1.1s	3.319%	1.2s
Regret Pred	SL Regret	✓	Guided LS (t=1s)	<b>0.098%</b>	1.1s	<b>1.049%</b>	1.4s
Edge Pred	SL	✗	Random + MCTS	0.002%	62.5ms	0.001%	0.4s
Regret Pred	SL Regret	✓	Random + MCTS	<b>0.000%</b>	0.2s	<b>0.179%</b>	1.8s
Sequential	RL	✗	Sampling	5.238%	11.4ms	9.364%	94.5ms
Sequential	Meta + RL	✓	Sampling	<b>2.157%</b>	72.7ms	<b>4.885%</b>	0.1s
Sequential	RL	✗	AS+Sampling	3.086%	3.2s	4.234%	6.7s
Sequential	Meta + RL	✓	AS+Sampling	<b>0.823%</b>	4.9s	<b>2.089%</b>	9.3s

#### 4.4 STREAMLINING THE ML4TSP DESIGN SPACE DISCOVERS MORE POWERFUL SOLVERS

This section investigates **Q2&3** by exploring potential recomposition among separable components in our framework, with the full results presented in Appendix Table 9.

**Evaluation of Heuristic Search.** We categorize search strategies outside learning as a construction-improvement paradigm, where constructive search and improvement-based search are orthogonal and can be combined. Table 9 shows that the most proper heuristic search strategy varies depending on the specific learning functionalities and objectives. Interestingly, even the more intricate MCTS method does not necessarily yield the best performance. [In cases where the output heatmap closely approximates feasible solutions and exhibits high discreteness \(e.g. the solution distribution proximity objective\), the effectiveness of utilizing the heatmap to guide the improvement search often falls short when compared to methods with smoother and more continuous heatmaps \(e.g. supervised solution proximity and meta reinforcement objectives for edge prediction\).](#) Due to space limitation, Table 6 adopts the fundamental solution proximity objective for edge prediction as an example to illustrate the effectiveness and recomposing performance of heuristic search methods implemented in our framework. The decoupled improvement MCTS can be combined with other construction methods to form variants like *Greedy\_MCTS*, *Sampling\_MCTS*, *Beam\_MCTS*, and *Random\_MCTS*, which utilize different constructive search for MCTS initialization, showing improvement in both solving performance and efficiency compared to the original MCTS solver (Fu et al., 2021). We use different time slices for varying problem scales, with the time for a single time slice denoted as  $t$ . We control the search process of MCTS by adjusting the number of time slices. More details are given in Appendix E.3.

**Recomposing to the Optimal.** We recombine the learning and search techniques in our framework to produce a factory of solvers. Table 7 presents the best three method combinations for every learning functionality. The recomposed solvers achieve SOTA performance that reaches 0.000% for TSP-50, 0.001% for TSP-100, and 0.142% for TSP-500. We find that top-performing methods remain closely tied to robust search such as MCTS, while generative models, specifically diffusion

Table 7: Optimal recombination of learning and search techniques. \*: reference for drop estimation.

Training Stage		Solving Stage			TSP-50		TSP-100		TSP-500	
Learning Functionality	Training Objective	Learning Search	Construction	Impr. Search	Drop↓	Time	Drop↓	Time	Drop↓	Time
-	-	-	PyConcorde (Applegate et al., 2006)	-	0.000±0.000%	73.6ms	0.000±0.000%	0.4s	0.000±0.000%	18.7s
-	-	-	LKH3 (trials=50) (Helsgaun, 2017)	-	0.000±0.000%	0.2s	0.002±0.019%	0.2s	0.322±0.174%	0.7s
-	-	-	LKH3 (trials=5k) (Helsgaun, 2017)	-	-	-	0.000±0.006%	1.6s	0.072±0.078%	4.2s
-	-	-	LKH3 (trials=50k) (Helsgaun, 2017)	-	-	-	-	-	0.014±0.029%	26.3s
Edge Pred	SL + Node Norm	-	Greedy	MCTS	0.021±0.114%	7.4ms	0.080±0.261%	16.3ms	0.578±0.420%	1.3s
Edge Pred	SL	-	Random (n=50)	MCTS	0.002±0.025%	62.5ms	<b>0.001±0.012%</b>	0.4s	0.301±0.153%	55.2s
Edge Pred.	SL + Node Norm	-	Random (n=50)	MCTS	0.004±0.026%	50.4ms	0.002±0.018%	0.4s	<b>0.142±0.106%</b>	55.3s
Regret Pred	SL Regret	-	Greedy	Guided LS (l=10s)	0.004±0.035%	10.1s	0.483±0.901%	10.4s	-	-
Regret Pred	SL Regret	-	MCTS Solver (100)	-	0.001±0.022%	63.4ms	1.116±0.781%	0.2s	-	-
Regret Pred	SL Regret	-	Random (n=50)	MCTS	<b>0.000±0.000%</b>	0.2s	0.179±0.241%	1.8s	-	-
Generation	Generative + Sym.	-	Greedy	Two-Opt	0.046±0.140%	0.2s	0.077±0.160%	0.4s	0.794±0.553%	1.6s
Generation	Generative + Sym.	Gradient Search	Greedy	Two-Opt	0.012±0.053%	0.7s	0.023±0.068%	0.8s	0.442±0.253%	3.8s
Generation	Generative + Sym.	Gradient Search	8× Greedy	Two-Opt	0.002±0.024%	1.3s	0.003±0.022%	5.0s	0.188±0.138%	28.6s
Sequential	RL	-	Sampling + Multistart	-	0.156±0.265%	1.3ms	1.618±0.893%	1.6ms	-	-
Sequential	RL + Sym. Baseline	-	Greedy + Multistart	Two-Opt	0.122±0.244%	0.1s	0.706±0.548%	0.5s	-	-
Sequential	RL + Sym. Baseline	-	Sampling + Multistart	Two-Opt	0.110±0.242%	0.2s	0.729±0.533%	1.5s	-	-

Table 8: Generalization Results with models trained on TSP-500. \*: reference for drop estimation.

Training Stage		Solving Stage			TSP-1000		TSPLIB 200-1000	
Learning Functionality	Training Objective	Learning Search	Construction	Impr. Search	Drop↓	Time	Drop↓	Time
-	-	-	PyConcorde (Applegate et al., 2006)	-	0.000%	84.4s	0.000%	10.6s
Edge Pred.	SL	-	Greedy	MCTS	1.171%	6.0s	1.416%	1.8s
Edge Pred.	SL + Node Norm	-	Greedy	MCTS	0.798%	6.1s	1.252%	1.8s
Edge Pred.	SL + Node Norm	-	Sampling (n=10)	MCTS	0.687%	83.5s	<b>0.517%</b>	17.9s
Edge Pred.	SL + Node Norm	-	Random (n=10)	MCTS	<b>0.603%</b>	54.6s	0.678%	17.3s
Solution Generation	Generative	-	Greedy	Two-Opt	1.811%	2.3s	2.431%	1.6s
Solution Generation	Generative + Sym.	-	Greedy	Two-Opt	1.735%	1.9s	1.880%	1.7s
Solution Generation	Generative + Sym.	Gradient Search	Greedy	Two-Opt	1.293%	6.1s	1.337%	4.4s
Solution Generation	Generative + Sym.	-	8× Greedy	Two-Opt	1.153%	22.4s	1.013%	5.8s

models, excel in constructive solvers without heavy reliance on heavy search, achieving 0.002%, 0.003%, 0.188% for TSP-50, 100 and 500. This highlights the potential for future development of more powerful solvers grounded in generative objectives and diffusion backbones. Considering the trade-off between solution quality and solving time, the best solutions are often achieved at the cost of higher computational expense. For comprehensiveness, Table 7 has also selected, for each learning functionality, recompositions at different speed levels, including the fastest approach with stable solution quality for demonstration. This is to accommodate scenarios that prioritize speed or approximation quality over strict optimality, where RL methods stand out with the fastest speed.

**Evaluation for Generalization.** We reconduct ablations over top-performing models to verify the generalization performance of the framework and whether the claims still hold for generalization to larger scale TSP, i.e., TSP-1000, and TSPLIB instances with 200-1000 nodes. The verified models are trained on TSP-500. Comparing methods in Table 8, we observe that the advantages of design principles such as joint probability estimation, symmetry solution representation, online optimization, and search friendliness persist across generalization. Additionally, the newly recomposed search method, *Random\_MCTS*, continues to demonstrate a performance advantage in generalization.

Regarding problem size, as observed in Table 9, the general trend is that the larger the scale, the worse the model’s relative solving performance. This is due to the increased difficulty of larger-scale problems. Additionally, we find that learning strategies that play supportive roles (e.g., guiding MCTS) are less scale-sensitive, while end-to-end methods (e.g., generative and RL) are more affected. This may be because strong search methods mitigate the risk of reduced prediction quality by learning. However, we can also see that methods like generative models still perform well as the scale increases due to their strong model expressiveness. On the other hand, when considering model complexity and training time, we find that methods with shorter training times, like unsupervised learning, are relatively less affected by scale. This may be because the bottleneck is the model capacity or the amount of learnable information using UL rather than task difficulty.

## 5 CONCLUSION

We design a principled modular framework that integrates existing ML4TSP practices, allowing for inspecting the current system. Based on this unification, we analyze the relationship between learning and solving objectives and show that learning generally improves solving with compatible search algorithms. We also analyze the effectiveness of current ML4TSP efforts, identifying desirable design principles for ML solvers like joint probability estimation, symmetry solution representation, and online optimization. Additionally, we offer insights into how model predictions intervene with strong search methods like MCTS and highlight preferences in learning paradigms for ML4TSP. Leveraging our findings, we propose enhancements to existing methods to compensate for their missing attributes and recombine within the established technique library to establish a factory of learning-based solvers, among which the optimal compositions achieve clear performance gains. Our implementation is carefully organized, facilitating easy development for further research and engineering practices.

## 540 ETHICS STATEMENT

541

542 This research complies with ethical standards, utilizing datasets that are either synthetic or publicly  
 543 available and contain no sensitive or personally identifiable information. It involves no direct human  
 544 subjects, nor does it present privacy or security concerns. All methodologies and experiments were  
 545 conducted in line with legal regulations and established research integrity practices. There are no  
 546 conflicts of interest, external sponsorship influences, or concerns regarding discrimination, bias, or  
 547 fairness. Moreover, the research does not lead to any harmful insights or applications.

548

## 549 REPRODUCIBILITY STATEMENT

550

551 We have taken steps to ensure the reproducibility of the results presented in this paper. The ex-  
 552 perimental settings, including datasets and model designs, are thoroughly described in Section 4.  
 553 Additional details, such as algorithm details and model configurations, are provided in Appendix E.  
 554 We provide full records of our experiments in Table 9 and provide minimalistic code example for the  
 555 implementation in Appendix C. Source code will be made publicly available upon acceptance.

556

## 557 REFERENCES

558

559 SP Anbuudayasankar, K Ganesh, Sanjay Mohapatra, SP Anbuudayasankar, K Ganesh, and Sanjay  
 560 Mohapatra. Survey of methodologies for tsp and vrp. *Models for Practical Routing Problems in  
 561 Logistics: Design and Practices*, pp. 11–42, 2014.

562 David Applegate, Ribert Bixby, Vasek Chvatal, and William Cook. Concorde tsp solver, 2006.

563

564 Jacob Austin, Daniel D Johnson, Jonathan Ho, Daniel Tarlow, and Rianne van den Berg. Structured  
 565 denoising diffusion models in discrete state-spaces. *Advances in Neural Information Processing  
 566 Systems*, 34:17981–17993, 2021.

567

568 Yoshua Bengio, Andrea Lodi, and Antoine Prouvost. Machine learning for combinatorial optimization:  
 569 a methodological tour d’horizon. *European Journal of Operational Research*, 2021.

570 Federico Berto, Chuanbo Hua, Junyoung Park, Minsu Kim, Hyeonah Kim, Jiwoo Son, Haeyeon  
 571 Kim, Joungho Kim, and Jinkyoo Park. R14co: a unified reinforcement learning for combinatorial  
 572 optimization library. In *NeurIPS 2023 Workshop: New Frontiers in Graph Learning*, 2023.

573

574 Lorenzo Brusca, Lars CPM Quaedvlieg, Stratis Skoulakis, Grigorios Chrysos, and Volkan Cevher.  
 575 Maximum independent set: self-training through dynamic programming. *Advances in Neural  
 576 Information Processing Systems*, 36:40637–40658, 2023.

577 Quentin Cappart, Didier Chételat, Elias Khalil, Andrea Lodi, Christopher Morris, and Petar  
 578 Veličković. Combinatorial optimization and reasoning with graph neural networks. *arXiv preprint  
 579 arXiv:2102.09544*, 2021.

580

581 Omar Cheikhrouhou and Ines Khoufi. A comprehensive survey on the multiple traveling salesman  
 582 problem: Applications, approaches and taxonomy. *Computer Science Review*, 40:100369, 2021.

583 Paulo R de O da Costa, Jason Rhuggenaath, Yingqian Zhang, and Alp Akcay. Learning 2-opt  
 584 heuristics for the traveling salesman problem via deep reinforcement learning. *arXiv preprint  
 585 arXiv:2004.01608*, 2020.

586

587 Chelsea Finn, Pieter Abbeel, and Sergey Levine. Model-agnostic meta-learning for fast adaptation of  
 588 deep networks. In *International conference on machine learning*, pp. 1126–1135. PMLR, 2017.

589 Zhang-Hua Fu, Kai-Bin Qiu, and Hongyuan Zha. Generalize a small pre-trained model to arbitrarily  
 590 large tsp instances. In *Proceedings of the AAAI Conference on Artificial Intelligence*, 2021.

591

592 Katayoon Goshvadi, Haoran Sun, Xingchao Liu, Azade Nova, Ruqi Zhang, Will Grathwohl, Dale  
 593 Schuurmans, and Hanjun Dai. Discs: a benchmark for discrete sampling. *Advances in Neural  
 Information Processing Systems*, 36, 2024.

- 594 Keld Helsgaun. An extension of the lin-kernighan-helsgaun tsp solver for constrained traveling  
595 salesman and vehicle routing problems. *Roskilde: Roskilde University*, pp. 24–50, 2017.  
596
- 597 Jonathan Ho, Ajay Jain, and Pieter Abbeel. Denoising diffusion probabilistic models. *Advances in*  
598 *Neural Information Processing Systems*, 33:6840–6851, 2020.
- 599 André Hottung, Bhanu Bhandari, and Kevin Tierney. Learning a latent search space for routing  
600 problems using variational autoencoders. In *International Conference on Learning Representations*,  
601 2021a.
- 602 André Hottung, Yeong-Dae Kwon, and Kevin Tierney. Efficient active search for combinatorial  
603 optimization problems. In *International Conference on Learning Representations*, 2021b.  
604
- 605 Qingchun Hou, Jingwei Yang, Yiqiang Su, Xiaoqing Wang, and Yuming Deng. Generalize learned  
606 heuristics to solve large-scale vehicle routing problems in real-time. In *The Eleventh International*  
607 *Conference on Learning Representations*, 2023.
- 608 Benjamin Hudson, Qingbiao Li, Matthew Malencia, and Amanda Prorok. Graph neural network  
609 guided local search for the traveling salesperson problem. *arXiv preprint arXiv:2110.05291*, 2021.  
610
- 611 Benjamin Hudson, Qingbiao Li, Matthew Malencia, and Amanda Prorok. Graph neural network  
612 guided local search for the traveling salesperson problem. In *International Conference on Learning*  
613 *Representations*, 2022. URL <https://openreview.net/forum?id=ar92oEosBIg>.
- 614 Chaitanya K Joshi, Thomas Laurent, and Xavier Bresson. An efficient graph convolutional network  
615 technique for the travelling salesman problem. *arXiv preprint arXiv:1906.01227*, 2019.  
616
- 617 Chaitanya K Joshi, Quentin Cappart, Louis-Martin Rousseau, and Thomas Laurent. Learning the  
618 travelling salesperson problem requires rethinking generalization. *arXiv preprint arXiv:2006.07054*,  
619 2020.
- 620 Nikolaos Karalias and Andreas Loukas. Erdos goes neural: an unsupervised learning framework for  
621 combinatorial optimization on graphs. *Advances in Neural Information Processing Systems*, 33:  
622 6659–6672, 2020.
- 623 Elias Khalil, Hanjun Dai, Yuyu Zhang, Bistra Dilkina, and Le Song. Learning combinatorial  
624 optimization algorithms over graphs. *Advances in neural information processing systems*, 30,  
625 2017.  
626
- 627 Minjun Kim, Junyoung Park, and Jinkyoo Park. Learning to cross exchange to solve min-max vehicle  
628 routing problems. In *The Eleventh International Conference on Learning Representations*, 2023.
- 629 Minsu Kim, Junyoung Park, and Jinkyoo Park. Sym-nco: Leveraging symmetricity for neural  
630 combinatorial optimization. *arXiv preprint arXiv:2205.13209*, 2022.  
631
- 632 Thomas N Kipf and Max Welling. Semi-supervised classification with graph convolutional networks.  
633 *arXiv preprint arXiv:1609.02907*, 2016.
- 634 Wouter Kool, Herke Van Hoof, and Max Welling. Attention, learn to solve routing problems! *arXiv*  
635 *preprint arXiv:1803.08475*, 2018.  
636
- 637 Yeong-Dae Kwon, Jinho Choo, Byoungjip Kim, Iljoo Yoon, Youngjune Gwon, and Seungjai Min.  
638 Pomo: Policy optimization with multiple optima for reinforcement learning. *Advances in Neural*  
639 *Information Processing Systems*, 33:21188–21198, 2020.
- 640 Sebastian Lamm, Peter Sanders, Christian Schulz, Darren Strash, and Renato F Werneck. Finding  
641 near-optimal independent sets at scale. In *2016 Proceedings of the eighteenth workshop on*  
642 *algorithm engineering and experiments (ALENEX)*, pp. 138–150. SIAM, 2016.
- 643 Yang Li, Jinpei Guo, Runzhong Wang, and Junchi Yan. T2t: From distribution learning in training  
644 to gradient search in testing for combinatorial optimization. In *Advances in Neural Information*  
645 *Processing Systems*, 2023.  
646
- 647 Shen Lin and Brian W Kernighan. An effective heuristic algorithm for the traveling-salesman problem.  
*Operations research*, 21(2):498–516, 1973.

- 648 Fu Luo, Xi Lin, Fei Liu, Qingfu Zhang, and Zhenkun Wang. Neural combinatorial optimization with  
649 heavy decoder: Toward large scale generalization. *arXiv preprint arXiv:2310.07985*, 2023.
- 650  
651 Fu Luo, Xi Lin, Fei Liu, Qingfu Zhang, and Zhenkun Wang. Neural combinatorial optimization with  
652 heavy decoder: Toward large scale generalization. *Advances in Neural Information Processing  
653 Systems*, 36, 2024.
- 654 Yining Ma, Zhiguang Cao, and Yeow Meng Chee. Learning to search feasible and infeasible regions  
655 of routing problems with flexible neural k-opt. *Advances in Neural Information Processing Systems*,  
656 36, 2024.
- 657  
658 Rajesh Matai, Surya Prakash Singh, and Murari Lal Mittal. Traveling salesman problem: an overview  
659 of applications, formulations, and solution approaches. *Traveling salesman problem, theory and  
660 applications*, 1(1):1–25, 2010.
- 661 Yimeng Min, Yiwei Bai, and Carla P Gomes. Unsupervised learning for solving the travelling  
662 salesman problem. *arXiv preprint arXiv:2303.10538*, 2023.
- 663  
664 Yuichi Nagata and Shigenobu Kobayashi. A powerful genetic algorithm using edge assembly  
665 crossover for the traveling salesman problem. *INFORMS Journal on Computing*, 25(2):346–363,  
666 2013.
- 667 Alex Nowak, Soledad Villar, Afonso S Bandeira, and Joan Bruna. A note on learning algorithms  
668 for quadratic assignment with graph neural networks. In *Proceeding of the 34th International  
669 Conference on Machine Learning (ICML)*, volume 1050, pp. 22, 2017.
- 670  
671 Yun Peng, Byron Choi, and Jianliang Xu. Graph learning for combinatorial optimization: A survey  
672 of state-of-the-art. *Data Science and Engineering*, 6(2):119–141, 2021.
- 673  
674 Petrică C Pop, Ovidiu Cosma, Cosmin Sabo, and Corina Pop Sitar. A comprehensive survey on the  
675 generalized traveling salesman problem. *European Journal of Operational Research*, 2023.
- 676  
677 Ruizhong Qiu, Zhiqing Sun, and Yiming Yang. Dimes: A differentiable meta solver for combinatorial  
678 optimization problems. *arXiv preprint arXiv:2210.04123*, 2022.
- 679 Sebastian Sanokowski, Wilhelm Franz Berghammer, Sepp Hochreiter, and Sebastian Lehner. Varia-  
680 tional annealing on graphs for combinatorial optimization. In *Thirty-seventh Conference on Neural  
681 Information Processing Systems*, 2023.
- 682 David Silver, Aja Huang, Chris J Maddison, Arthur Guez, Laurent Sifre, George Van Den Driessche,  
683 Julian Schrittwieser, Ioannis Antonoglou, Veda Panneershelvam, Marc Lanctot, et al. Mastering  
684 the game of go with deep neural networks and tree search. *nature*, 529(7587):484–489, 2016.
- 685  
686 Jiaming Song, Chenlin Meng, and Stefano Ermon. Denoising diffusion implicit models. *arXiv  
687 preprint arXiv:2010.02502*, 2020.
- 688  
689 Zhiqing Sun and Yiming Yang. Difusco: Graph-based diffusion solvers for combinatorial optimization.  
690 *arXiv preprint arXiv:2302.08224*, 2023.
- 691  
692 Petar Veličković, Guillem Cucurull, Arantxa Casanova, Adriana Romero, Pietro Lio, and Yoshua  
693 Bengio. Graph attention networks. *arXiv preprint arXiv:1710.10903*, 2017.
- 694  
695 Thibaut Vidal. Hybrid genetic search for the cvrp: Open-source implementation and swap\* neighbor-  
696 hood. *Computers & Operations Research*, 140:105643, 2022.
- 697  
698 Oriol Vinyals, Meire Fortunato, and Navdeep Jaitly. Pointer networks. *Advances in neural information  
699 processing systems*, 28, 2015.
- 700  
701 Haoyu Wang and Pan Li. Unsupervised learning for combinatorial optimization needs meta-learning.  
*arXiv preprint arXiv:2301.03116*, 2023.
- Haoyu Peter Wang and Pan Li. Unsupervised learning for combinatorial optimization needs meta  
learning. In *The Eleventh International Conference on Learning Representations*, 2022.

702 Haoyu Peter Wang, Nan Wu, Hang Yang, Cong Hao, and Pan Li. Unsupervised learning for  
703 combinatorial optimization with principled objective relaxation. In *Advances in Neural Information*  
704 *Processing Systems*, 2022.

705 Runzhong Wang, Yunhao Zhang, Ziao Guo, Tianyi Chen, Xiaokang Yang, and Junchi Yan. Linsatnet:  
706 the positive linear satisfiability neural networks. In *International Conference on Machine Learning*,  
707 pp. 36605–36625. PMLR, 2023.

708 Frederik Wenkel, Yimeng Min, Matthew Hirn, Michael Perlmutter, and Guy Wolf. Overcoming  
709 oversmoothness in graph convolutional networks via hybrid scattering networks. *arXiv preprint*  
710 *arXiv:2201.08932*, 2022.

711 Ronald J Williams. Simple statistical gradient-following algorithms for connectionist reinforcement  
712 learning. *Machine learning*, 8:229–256, 1992.

713 Yingqian Zhang, Laurens Bliet, Paulo da Costa, Reza Refaei Afshar, Robbert Reijnen, Tom Catshoek,  
714 Daniël Vos, Sicco Verwer, Fynn Schmitt-Ulms, André Hottung, et al. The first ai4tsp competition:  
715 Learning to solve stochastic routing problems. *Artificial Intelligence*, 319:103918, 2023.

716 Jianan Zhou, Yaixin Wu, Wen Song, Zhiguang Cao, and Jie Zhang. Towards omni-generalizable  
717 neural methods for vehicle routing problems. In *International Conference on Machine Learning*,  
718 pp. 42769–42789. PMLR, 2023.

719  
720  
721  
722  
723  
724  
725  
726  
727  
728  
729  
730  
731  
732  
733  
734  
735  
736  
737  
738  
739  
740  
741  
742  
743  
744  
745  
746  
747  
748  
749  
750  
751  
752  
753  
754  
755

Table 9: Full Results of Learning and Searching Technique Recomposition for ML4TSP Solvers.

Method	Training Stage		Solving Stage			TSP-50			TSP-100			TSP-500		
	Training Objective	Learning Search	Construction	Impr. Search	Length	Drop	Time	Length	Drop	Time	Length	Drop	Time	
<i>Traditional Solver</i>														
Concorde (Applegate et al., 2006)	-	-	-	-	5.688*	0.000%	73.6ms	7.756*	0.000%	0.404s	16.546*	0.000%	18.672s	
Greedy	-	-	-	-	7.014	23.301%	0.31ms	9.680	24.798%	1.15ms	20.808	25.766%	35.84ms	
Insertion	-	-	-	-	6.126	7.708%	0.15ms	8.508	9.699%	0.28ms	18.608	12.461%	5.75ms	
GAX (Nguyen & Kraussbach, 2013)	-	-	-	-	5.688	0.000%	0.10s	7.756	0.000%	0.18s	16.546	0.001%	1.86s	
LKH3 (trials=5k) (Helsgaun, 2017)	-	-	-	-	5.688	0.000%	0.177s	7.756	0.002%	0.216s	16.599	0.322%	0.703s	
LKH3 (trials=5k) (Helsgaun, 2017)	-	-	-	-	-	-	-	7.756	0.000%	1.561s	16.558	0.072%	4.172s	
LKH3 (trials=50k) (Helsgaun, 2017)	-	-	-	-	-	-	-	-	-	16.548	0.014%	26.344s		
<i>Edge Prediction</i>														
GCN (Joshi et al., 2019)	SL	-	Greedy	-	5.776	1.530%	7.6ms	8.307	7.078%	10.6ms	18.571	12.237%	0.111s	
ML4TSP	SL	-	Greedy	Two-Opt	5.694	0.115%	7.6ms	7.806	0.649%	12.0ms	16.891	2.089%	0.128s	
ML4TSP	SL	-	Greedy	Guided LS (n=1)	5.723	0.614%	1.084s	8.014	3.319%	1.236s	17.818	7.682%	45.469s	
ML4TSP	SL	-	Greedy	-	5.689	0.018%	8.4ms	7.768	0.154%	16.8ms	16.684	0.838%	1.320s	
GCN (Joshi et al., 2019)	SL	-	Beam (n=1280)	Two-Opt	5.689	0.023%	1.099s	7.808	0.673%	2.320s	20.456	23.629%	11.602s	
ML4TSP	SL	-	Random (n=10)	MCTS	5.688	0.015%	1.099s	7.767	0.149%	2.323s	16.948	2.431%	12.859s	
ML4TSP	SL	-	Beam (n=10)	MCTS	5.688	0.008%	38.8ms	7.758	0.027%	0.102s	16.609	0.380%	11.409s	
ML4TSP	SL	-	Beam (n=20)	MCTS	5.688	0.006%	54.9ms	7.757	0.014%	0.176s	16.598	0.315%	22.712s	
ML4TSP	SL	-	Beam (n=50)	MCTS	5.688	0.005%	0.111s	7.757	0.009%	0.475s	16.585	0.235%	56.286s	
ML4TSP	SL	-	Sampling (n=10)	MCTS	5.688	0.005%	37.5ms	7.756	0.008%	0.124s	16.645	0.907%	11.788s	
ML4TSP	SL	-	Sampling (n=20)	MCTS	5.688	0.004%	61.5ms	7.756	0.004%	0.280s	16.630	0.509%	23.338s	
ML4TSP	SL	-	Sampling (n=50)	MCTS	5.688	0.002%	0.114s	7.756	0.001%	0.549s	16.611	0.396%	58.122s	
ML4TSP	SL	-	Random (n=10)	MCTS	5.688	0.014%	17.5ms	7.757	0.011%	81.4ms	16.632	0.519%	11.159s	
ML4TSP	SL	-	Random (n=20)	MCTS	5.688	0.003%	28.7ms	7.756	0.003%	0.155s	16.616	0.422%	22.131s	
ML4TSP	SL	-	Random (n=50)	MCTS	5.688	0.002%	62.5ms	7.756	0.001%	0.374s	16.596	0.301%	55.195s	
Ant-GCN (Fu et al., 2021)	SL	-	MCTS Solver (1)	-	5.688	0.009%	11.7ms	7.759	0.035%	29.9ms	16.704	0.958%	1.078s	
Ant-GCN (Fu et al., 2021)	SL	-	MCTS Solver (5)	-	5.688	0.007%	31.7ms	7.757	0.009%	0.118s	16.634	0.536%	5.082s	
Ant-GCN (Fu et al., 2021)	SL	-	MCTS Solver (10)	-	5.688	0.006%	56.7ms	7.756	0.006%	0.217s	16.617	0.433%	10.081s	
ML4TSP	SL + Node Norm	-	Greedy	-	5.727	0.674%	7.4ms	7.968	2.721%	10.1ms	17.952	8.496%	0.111s	
ML4TSP	SL + Node Norm	-	Greedy	Two-Opt	5.692	0.082%	7.4ms	7.779	0.292%	11.7ms	16.765	1.325%	0.128s	
ML4TSP	SL + Node Norm	-	MCTS	-	5.689	0.021%	7.4ms	7.762	0.009%	16.3ms	16.641	0.295%	1.297s	
ML4TSP	SL + Node Norm	-	Beam (n=1280)	-	5.688	0.016%	1.132s	7.798	0.545%	2.241s	20.133	21.678%	13.720s	
ML4TSP	SL + Node Norm	-	Beam (n=1280)	Two-Opt	5.688	0.012%	1.142s	7.768	0.156%	2.254s	16.908	2.189%	14.009s	
ML4TSP	SL + Node Norm	-	Beam (n=10)	MCTS	5.688	0.012%	28.1ms	7.758	0.027%	98.6ms	16.585	0.238%	11.413s	
ML4TSP	SL + Node Norm	-	Beam (n=20)	MCTS	5.688	0.011%	56.7ms	7.757	0.019%	0.179s	16.580	0.208%	22.652s	
ML4TSP	SL + Node Norm	-	Beam (n=50)	MCTS	5.688	0.008%	94.5ms	7.757	0.013%	0.421s	16.571	0.152%	56.094s	
ML4TSP	SL + Node Norm	-	Sampling (n=10)	MCTS	5.688	0.009%	28.1ms	7.757	0.011%	0.108s	16.590	0.265%	11.882s	
ML4TSP	SL + Node Norm	-	Sampling (n=20)	MCTS	5.688	0.008%	0.207s	7.756	0.005%	0.271s	16.581	0.214%	55.284s	
ML4TSP	SL + Node Norm	-	Sampling (n=50)	MCTS	5.688	0.006%	0.115s	7.756	0.003%	0.529s	16.569	0.142%	59.119s	
ML4TSP	SL + Node Norm	-	Random (n=10)	MCTS	5.688	0.007%	16.5ms	7.756	0.009%	81.5ms	16.586	0.245%	11.844s	
ML4TSP	SL + Node Norm	-	Random (n=20)	MCTS	5.688	0.004%	27.7ms	7.756	0.004%	0.156s	16.579	0.200%	22.308s	
ML4TSP	SL + Node Norm	-	Random (n=50)	MCTS	5.688	0.002%	64.8ms	7.756	0.002%	0.389s	16.569	0.142%	59.244s	
ML4TSP	SL + Node Norm	-	MCTS Solver (10)	-	5.688	0.010%	56.7ms	7.760	0.013%	0.210s	16.600	0.329%	10.188s	
ML4TSP	UL	-	Greedy	-	6.405	12.600%	11.4ms	8.870	14.360%	17.0ms	-	-	-	
ML4TSP	UL	-	Greedy	Two-Opt	5.846	2.785%	12.8ms	8.003	3.182%	35.0ms	-	-	-	
ML4TSP	UL	-	Greedy	MCTS	5.863	3.096%	28.9ms	8.069	4.039%	89.0ms	-	-	-	
UTSP (Min et al., 2023)	UL	-	MCTS Solver (10)	-	5.818	2.300%	62.9ms	8.069	4.463%	0.223s	-	-	-	
ML4TSP	RL	-	Sampling	-	5.985	5.238%	11.4ms	8.481	9.364%	94.5ms	19.296	16.612%	1.039s	
ML4TSP	RL	Active Search	Sampling	-	5.863	3.086%	3.24s	8.084	4.234%	6.703s	17.865	7.959%	258.281s	
DIMES (Qiu et al., 2022)	Meta + RL	-	Greedy	-	6.360	11.847%	15.6ms	8.790	13.339%	18.0ms	19.605	18.489%	0.375s	
DIMES (Qiu et al., 2022)	Meta + RL	-	Sampling	-	5.933	4.310%	35.9ms	8.135	4.885%	0.124s	18.706	13.056%	1.305s	
DIMES (Qiu et al., 2022)	Meta + RL	-	MCTS Solver (10)	-	5.697	0.172%	60.6ms	7.807	0.661%	0.216s	17.425	5.318%	10.296s	
DIMES (Qiu et al., 2022)	Meta + RL	Active Search	Greedy	-	5.897	3.681%	4.23s	8.111	4.583%	8.575s	17.763	7.341%	264.781s	
DIMES (Qiu et al., 2022)	Meta + RL	Active Search	Sampling	-	5.859	3.006%	2.884s	8.061	3.940%	8.508s	17.694	6.924%	274.797s	
ML4TSP	Meta + RL	-	Greedy	Two-Opt	5.823	2.387%	18.0ms	8.007	3.232%	57.0ms	17.165	3.742%	0.453s	
ML4TSP	Meta + RL	-	Greedy	LS	6.016	5.756%	62.6ms	8.739	7.520%	0.457s	17.528	8.149%	48.688s	
ML4TSP	Meta + RL	-	Greedy	Guided LS (n=1)	5.986	5.231%	1.112s	8.335	7.463%	1.382s	17.938	8.408%	51.406s	
ML4TSP	Meta + RL	-	Greedy	MCTS	5.765	1.337%	18.8ms	7.909	1.973%	42.4ms	17.354	4.884%	1.385s	
ML4TSP	Meta + RL	-	Random (n=50)	MCTS	5.688	0.018%	0.241s	7.765	0.123%	1.522s	17.655	6.703%	59.297s	
ML4TSP	Meta + RL	-	Sampling	Two-Opt	5.791	1.821%	0.144s	7.979	2.880%	0.278s	16.578	0.238%	6.944s	
ML4TSP	Meta + RL	-	Sampling	Two-Opt	5.776	1.549%	4.414s	7.925	2.176%	8.859s	17.263	4.322%	277.031s	
ML4TSP	Meta + RL	Active Search	Sampling-RandStart	-	5.735	0.823%	4.862s	7.918	2.089%	9.330s	17.646	6.635%	272.813s	
<i>Edge Regret Prediction</i>														
ML4TSP	SL Regret	-	Greedy	-	6.179	8.651%	18.8ms	8.966	15.597%	16.4ms	-	-	-	
ML4TSP	SL Regret	-	Greedy	Two-Opt	5.707	0.333%	19.5ms	7.857	1.295%	0.129s	-	-	-	
ML4TSP	SL Regret	-	Guided LS	-	5.784	0.695%	0.064s	8.127	4.786%	0.306s	16.585	0.238%	10.417s	
GNGLS (Hudson et al., 2021)	SL Regret	-	Greedy	Guided LS (n=1s)	5.693	0.998%	1.080s	7.837	1.049%	1.389s	-	-	-	
GNGLS (Hudson et al., 2021)	SL Regret	-	Greedy	Guided LS (n=10s)	5.688	0.004%	10.078s	7.793	0.483%	10.359s	-	-	-	
ML4TSP	SL Regret	-	Greedy	MCTS	5.702	0.255%	17.2ms	7.927	2.210%	54.0ms	-	-	-	
ML4TSP	SL Regret	-	Random (n=50)	MCTS	5.688	0.000%	0.240s	7.770	0.199%	0.843s	-	-	-	
ML4TSP	SL Regret	-	MCTS Solver (10)	-	5.688	0.001%	63.4ms	7.823	1.116%	0.218s	-	-	-	
<i>Solution Generation</i>														
DIFUSCO (Sun & Yang, 2023)	Generative	-	Greedy	-	5.709	0.384%	0.388s	7.845	1.136%	0.409s	18.144	9.639%	1.188s	
DIFUSCO (Sun & Yang, 2023)	Generative	-	Greedy	Two-Opt	5.694	0.105%	0.394s	7.776	0.261%	0.409s	16.800	1.524%	1.203s	
DIFUSCO (Sun & Yang, 2023)	Generative	-	8 * Greedy	-	5.688	0.014%	0.688s	7.761	0.062%	2.355s	17.312	4.613%	6.867s	
DIFUSCO (Sun & Yang, 2023)	Generative	-	8 * Greedy	Two-Opt	5.688	0.010%	0.688s	7.759	0.035%	2.356s	16.662	0.686%	6.914s	
T2T (Li et al., 2023)	Generative	Gradient Search	Greedy	-	5.690	0.039%	1.164s	7.788	0.127%	1.198s	17.444	5.414%	2.805s	
T2T (Li et al., 2023)	Generative	Gradient Search	Greedy	Two-Opt	5.689	0.022%	1.181s	7.761	0.065%	1.217s	16.695	0.885%	2.836s	
ML4TSP	Generative + Sym.	-	Greedy	-	5.688	0.076%	0.225s	7.770	0.186%	0.398s	17.628	6.345%	1.578s	
ML4TSP	Generative + Sym.	-	Greedy	Two-Opt	5.690	0.046%	0.230s	7.762	0.077%	0.400s	16.680	0.811%	1.586s	
ML4TSP	Generative + Sym.	-	Greedy	MCTS	5.690	0.040%	0.318s	7.762	0.080%	0.489s	16.689	0.863%	1.716s	
ML4TSP	Generative + Sym.	-	8 * Greedy	-	5.688	0.007%	0.701s	7.757	0.011%	2.450s	16.790	1.476%	10.328s	
ML4TSP	Generative + Sym.	-	8 * Greedy	Two-Opt	5.688	0.006%	0.702s	7.757	0.009%	2.450s	16.585	0.303%	0.714s	
ML4TSP	Generative + Sym.	-	8 * Greedy	MCTS	5.688	0.006%	0.859s	7.757	0.009%	3.141s	16.605	0.357%	21.	

810 drops of 0.000%, 0.001%, and 0.142% on TSP of sizes 50, 100, and 500, respectively. 2) Without  
811 relying on tailored heuristics like MCTS, the generative distribution proximity objective based on the  
812 symmetry representation achieves the optimal results when adopting gradient search,  $8\times$  Greedy, and  
813 Two-Opt for the solving stage, achieving drops of 0.002%, 0.003%, and 0.188% on TSP of sizes 50,  
814 100, and 500, respectively. 3) Regarding the paradigms of learning-based solvers, we discover a clear  
815 performance advantage of non-autoregressive methods to autoregressive sequence models, and super-  
816 vised methods are significantly ahead of unsupervised methods, especially without the support of pow-  
817 erful heuristic search. For scalability, we notice that acquiring supervision for edge regret is extremely  
818 time-consuming, making it impractical for solving larger-scale problems like TSP-500. Meanwhile,  
819 RL-based sequence models also face challenges on larger-scale problems due to issues like sparse  
820 rewards and training instability, which also struggle to support training on larger-scale instances.

## 821 B ADAPTATION OF THE FRAMEWORK TO OTHER CO PROBLEMS

### 822 B.1 GUIDE FOR CROSS-PROBLEM ADAPTATION

823  
824 The ML field has gone the farthest optimizing the TSP, and we consider TSP as one of the most  
825 extensively studied CO problems with the richest learning and searching techniques. Note numerous  
826 methods have been devised in ML4CO. While some of the best-performing methods show promising  
827 results, they still exhibit a gap compared to traditional methods. The very first motivation of this work  
828 is to reassess the role of learning for CO (or specifically TSP) and to discern which parts of existing  
829 techniques are genuinely beneficial and which are not. For this purpose, we select TSP to incorporate  
830 and analyze learning and searching techniques as comprehensively as possible and, to the maximum  
831 extent, retain the potential for application to other problems.

832 This framework can be customized for other CO problems with the same modular organization and  
833 learning-based designs. The primary adaptations required would involve adjusting the optimization  
834 variables, e.g. replacing edges with nodes for node-decision problems such as Maximum Independent  
835 Set (MIS), as well as modifying the (optional) heuristic search designs that are problem-specific.  
836 Specifically, the pipeline for a new problem can be still generally be organized by a prediction-and-  
837 search pipeline like TSP, where the learning models can be trained with learning tasks including 1)  
838 decision variable prediction, 2) variable regret prediction, 3) solution generation, and 4) sequential  
839 variable prediction, as well as training objectives including 1) supervised solution proximity, 2)  
840 unsupervised solving objective, 3) reinforcement solving objective, 4) supervised variable regret  
841 proximity, 5) solution distribution proximity, potentially with the support of 6) meta learning objective.  
842 Then in the solving stage, the neural prediction can be further improved by learning-based search  
843 methods for specific problems, and the search phase can follow the construction-search pipeline with  
844 constructive search like Greedy and improvement-based search like local search.

845  
846 Additionally, many parts of our analysis, e.g., the study of the relationship between learning and  
847 solving objectives, the benefits of satisfying certain design principles like joint probability estimation,  
848 symmetry solution representation, online optimization, etc., indeed study the general learning designs  
849 and its synergy with search methods, maintaining the potential to have applicability beyond TSP  
850 in design. For example, for MIS, we can also consider achieving joint probability estimation by  
851 introducing a normalization term on the predicted node probabilities to enhance performance. For  
852 other problems with sequential solutions, we can consider enforcing the symmetry property for  
853 solution representations. In general pipeline designs, we can also consider introducing optimization  
854 during the testing phase to enhance performance.

855 **Meta Framework.** To facilitate adaptation to other CO problems, we have developed a task-agnostic  
856 skeleton and common toolkit, which provides robust support for the development of learning-based  
857 solvers across different tasks. This toolkit focuses on facilitating method development while leaving  
858 room for customizations of problem-specific implementations. Key features include:

- 859 1. A generic skeleton for organizing ML4CO frameworks;
- 860 2. Base classes to streamline method development;
- 861 3. Traditional solver baselines and reference solution acquisition;
- 862
- 863



- 864 4. Data generation for various distributions;
- 865 5. Problem and solution visualization tools;
- 866 6. Evaluators for multiple problem types;
- 867 7. Common post-processing algorithms.

870 This toolkit enables straightforward adaptation of our framework to new problems by inheriting base  
 871 classes and adhering to the pre-defined project structure. We extend our framework design to CVRP  
 872 and MIS problems, which include foundational classes for developing learning-based CVRP and  
 873 MIS solvers. These frameworks currently implement several popular learning-based solvers and can  
 874 be expanded to integrate additional methods using the same modular structure.

## 876 B.2 EMPIRICAL RESULTS

878 This subsection verifies the effectiveness of satisfying the discovered design principles in TSP to show  
 879 the reference value of the ML4TSP analysis to other CO problems. Here, we verify the Capacitated  
 880 Vehicle Routing Problem (VRP) and Maximum Independent Set (MIS) problems. Building upon the  
 881 principles, we introduce novel designs seamlessly integrated into existing pipelines to boost solving  
 882 performance and validate the effectiveness of adhering to these principles throughout the process.

### 884 B.2.1 EXPERIMENTAL SETUP

885 **CVRP Datasets.** Following Ma et al. (2024), we use samples with coordinates that are randomly  
 886 uniformly distributed, demands that are random integers between 1 and 9, and a total capacity of  
 887 40 as our training and testing sets. The training set size is 128000, with 100 training epochs. The  
 888 testing set size is 10000, consistent with Ma et al. (2024). Note that when using neural networks for  
 889 inference, the batch size is set to 100.

890 **CVRP Metrics.** We adopt three evaluation metrics to measure performance: 1) Length: the  
 891 average total distance of the solved tours w.r.t. the corresponding instances; 2) Drop: the relative  
 892 performance drop w.r.t. length compared to the nearly optimal solutions (obtained by the heuristic  
 893 solver HGS (Vidal, 2022) in this paper); 3) Time: the average computational time per instance.

894 **MIS Datasets.** We use SATLIB<sup>2</sup> as the dataset. Following Qiu et al. (2022); Sun & Yang (2023); Li  
 895 et al. (2023), we use 39500 samples as the training set and 500 samples as the test set.

897 **MIS Metrics.** Following Qiu et al. (2022); Sun & Yang (2023); Li et al. (2023), we adopt three  
 898 evaluation metrics to measure model performance: 1) Size: the average size of the solutions w.r.t.  
 899 the corresponding instances, i.e. the objective. 2) Drop: the relative performance drop w.r.t. size  
 900 compared to the nearly optimal solutions (obtained by the heuristic solver KaMIS (Lamm et al., 2016)  
 901 in this paper); 3) Time: the average computational time per instance.

### 903 B.2.2 JOINT PROBABILITY ESTIMATION HELPS CAPTURE VARIABLE CORRELATIONS

904 This subsection verifies whether the joint probability estimation property also benefits other CO  
 905 problems. Here, we adopt the MIS problem for evaluation. For MIS, the decision variable is the nodes  
 906 in the given graph. In the learning functionality of node prediction, the *SL* training objective generally  
 907 enforces supervision over each node’s binary classification results. This is based on the assumption  
 908 of mutual statistical independence of the individual solution parameters, such that the solution can  
 909 be represented by a product of Bernoulli distributions for the individual solution variables Sanokowski  
 910 et al. (2023). However, since the CO solutions are highly constrained with strong correlations among  
 911 the solution variables, such an assumption can lead to a performance drop.

912 With GNN raw predictions, which correspond to  $n$  nodes, prior methods utilize the softmax operation  
 913 over the last dimension to ensure that the probabilities of positive and negative edges sum up to 1.  
 914 The cross-entropy loss involves  $n$  nodes’ binary classification, lacking a general capture of joint  
 915 probability over the solution variables. To this end, we propose a relaxed probability normalization  
 916 term achieved by LinSAT layer Wang et al. (2023), which projects the raw predicted probabilities to

<sup>2</sup>[https://www.cs.ubc.ca/~hoos/SATLIB/Benchmarks/SAT/CBS/descr\\_CBS.html](https://www.cs.ubc.ca/~hoos/SATLIB/Benchmarks/SAT/CBS/descr_CBS.html)

the constrained space, where the positive node probabilities within each node’s adjacent node group to sum up to less than the size of the adjacent group minus one:

$$\sum_{j \in N(i)} p_j \leq |N(i)| - 1, \forall i \tag{6}$$

where  $N(i)$  denotes the adjacent node group (including itself) of node  $i$ , and  $p_j$  denotes the predicted probability for node  $j$ . This is a largely relaxed constraint for the MIS problem, yet it provides the chance to connect among the node probabilities.

Under the node prediction functionality, we also include methods of solution distribution proximity objective into comparison, which considers a solution as the whole entity, allowing it to naturally adhere to the joint probability distribution. Table 10 shows the ablation. Methods with joint probability estimation generally achieve lower drops.

Table 10: Joint probability estimation ablation based on methods with Variable Prediction as the learning functionality for MIS.

Objective	Joint Prob.	Solving Stage	SATLIB		
			Size↑	Drop↓	Time
KaMIS (10s) (Lamm et al., 2016)			425.954	0.000±0.000%	10s
SL	✗	Greedy	421.692	1.004±0.524%	22.7ms
SL + LinSAT Norm	✓	Greedy	422.098	0.907±0.473%	0.545s
Generative	✓	Greedy	424.496	0.344±0.329%	1.101s

### B.2.3 SYMMETRY SOLUTION REPRESENTATION INTRODUCES EQUIVALENCE AWARENESS

Similar to TSP, a CVRP tour holds symmetry or permutation invariance (Kwon et al., 2020). Since CO aims to produce optimal solutions, the neural model is expected to be aware of the equivalences among such sequences and should be optimized to consistently yield the same solution regardless of the variances in forms. This subsection endeavors to introduce the symmetry solution representation attribute to methods lacking symmetry consideration within the framework, thereby enhancing problem-solving performance.

For the *RL* objective, methods decode solutions sequentially during optimization. To achieve symmetry, we refer to Kwon et al. (2020) to optimize over diverse rollouts with multiple starting points as well as use symmetry baselines (Kim et al., 2022) for *Sequential* functionality. These techniques raise the model’s awareness of symmetry. Table 11 presents solving results on CVRP-50, showing a notable performance gain by introducing symmetry.

Table 11: Symmetry ablation based on methods with *RL* as the training objective on CVRP.

Functionality	Symmetry	Solving Stage	CVRP-50		
			Length↓	Drop↓	Time
HGS (1s) (Vidal, 2022)			10.366	0.000±0.000%	1.0s
Sequential	✗	Greedy	11.138	7.479±2.953%	0.9ms
+ MultiStart	✓	Greedy	10.605	2.305±1.184%	2.2ms
+ Sym. Baseline	✓	Greedy	10.989	6.035±2.613%	0.9ms
Sequential	✗	Sampling	11.201	8.093±3.187%	0.9ms
+ MultiStart	✓	Sampling	10.594	2.195±1.102%	2.2ms
+ Sym. Baseline	✓	Sampling	11.031	6.441±2.705%	0.9ms

### B.2.4 ONLINE OPTIMIZATION COMPLEMENTS GENERALIZATION CAPABILITY

In order to bridge the gap between training for average performance and solving for performance in new instances, instance-specific optimization can be helpful. We verify the effectiveness of techniques that optimize in the testing phase in Sec. 3.2.1: the gradient search for methods with *Generation* as the functionality. Table 12 ablates learning-based search, indicating a promising gain with learning-based search, however at the cost of additional computation.

Table 12: Ablation on online optimization property achieved by learning-based search on MIS.

Functionality	Objective	Solving Stage	SATLIB		
			Size↑	Drop↓	Time
Generation	Generative	Greedy	424.496	0.344±0.329%	1.101s
	Generative	Gradient Search + Greedy	425.006	0.224±0.213%	2.380s

### B.2.5 SEARCH FRIENDLINESS CONTRIBUTES TO LEARNING-SEARCH SYNERGY

Techniques that consider how to better integrate learning with search can benefit problem-solving. This subsection verifies the effectiveness of search friendliness designs by promoting diversity in the predicted solutions (e.g. modeling solution distribution) and incorporating the search process into optimization (e.g. through meta learning to learn optimal initialization for solving stage). For the effectiveness of prediction diversity, Table 13 demonstrates the improvement in solving performance achieved by adopting meta learning and employing multiple sampling, which is contributed by increased diversity.

Table 13: Ablation on search friendliness property on MIS.

Functionality	Objective	Search Frnd.	Solving Stage	SATLIB		
				Size↑	Drop↓	Time
Variable Prediction	RL	✗	Sampling	408.480	4.104±3.558%	27m34s
Variable Prediction	Meta + RL	✓	Sampling	410.596	3.607±2.864%	28m5s
Variable Prediction	Generative	✗	Greedy	424.496	0.344±0.329%	1.101s
Variable Prediction	Generative	✓	8×Greedy	425.142	0.192±0.198%	5.324s

## C MINIMALISTIC CODE EXAMPLE FOR ML4TSP SOLVERS

### C.1 TSPSOLVER

To accommodate diverse data types and facilitate the evaluation of solution quality, we provide a **TSPSolver** base class that offers a user-friendly approach for solving TSP. This class includes functionalities for data input and output, as well as an evaluation function. The solver supports different data inputs, such as Numpy arrays and *.txt* and *.tsp* files. The outputs can be saved to corresponding types of files as needed. Additionally, the solver offers an evaluation function, by which users can quickly obtain the average tour length, average gap, and standard deviation of the test dataset. Below is an example of using TSPSolver to obtain the average tour length of the LKH test dataset, as well as its gap with standard deviation relative to the Concorde test dataset.

```
>>> from ml4tsp import TSPSolver

# Read the test file
>>> solver = TSPSolver()
>>> solver.from_txt("dataset/tsp_uniform/tsp500_lkh.txt")
# Assign the ref_tour of the tested solver as the solution path
>>> solver.read_tours(solver.ref_tours)
# Read the reference file
>>> solver.from_txt("dataset/tsp_uniform/tsp500_concorde.txt")
# (costs_avg, ref_costs_avg, gap_avg, gap_std)
>>> lkh_solver.evaluate(calculate_gap=True)
(16.548110417020276, 16.545805334644392,
0.0139392061675804, 0.028643127914360397)
```

1026 C.2 LEARNING-BASED SOLVERS  
1027

1028 To enhance the modularization and cohesion within our proposed framework, we have extended the  
1029 **TSPSolver** base class to support two highly integrated learning-based solvers: **ML4TSPNARSolver**  
1030 and **ML4TSPARSolver**. These solvers can efficiently configure design choices and be called to solve  
1031 given instances. The following code snippet shows minimalistic code for TSP solving exemplified by  
1032 solution proximity objective with greedy and MCTS as heuristic search:

```
1033
1034 >>> from ml4tsp import ML4TSPGNNSSolver, ML4TSPNAREnv
1035
1036 # Create ML4TSPEnv
1037 >>> env = ML4TSPNAREnv(
1038     nodes_num=500, # the number of nodes
1039     sparse_factor=50 # KNN graph representation
1040 )
1041
1042 # Create Solver
1043 # If `pretrained` is True and `pretrained_path` is None,
1044 # ML4TSP will automatically download the corresponding
1045 # pre-trained file online.
1046 >>> solver = ML4TSPGNNSSolver(
1047     env=env,
1048     encode_device="cuda",
1049     decoder="random",
1050     decoder_kwargs={"samples_num": 50},
1051     local_search="mcts",
1052     local_search_kwargs={"time_limit": 1.0},
1053     local_search_device="cpu",
1054     scale=1,
1055     pretrained=True,
1056     pretrained_path="weights/tsp500_gnn.pt"
1057 )
1058
1059 # Read data
1060 >>> solver.from_txt("dataset/tsp_uniform/tsp500_test.txt")
1061
1062 # Solve
1063 >>> solver.solve(batch_size=1)
1064
1065 Encoding: 100%|----| 128/128 [00:05<00:00, 25.23it/s]
1066 Encode Time: 9.426303148269653
1067 Decoding: 100%|----| 128/128 [00:00<00:00, 650.48it/s]
1068 Decode Time: 1.578188419342041
1069 Local Search: 100%|----| 6400/6400 [1:57:33<00:00, 1.10s/it]
1070 Local Search Time: 7054.012353181839
1071
1072 # Using the evaluate function to obtain result
1073 >>> solver.evaluate(calculate_gap=True)
1074 (16.59568398521005, 16.545805334644392,
1075 0.3014236256908176, 0.15272430899596431)
1076
1077 # Output and Save the solution results
1078 >>> solver.to_txt("tsp500_gnn_random50_mcts.txt")
1079
```

### 1080 C.3 TSPLKHSOLVER AND TSPCONCORDESOLVER

1081  
1082 In order to make the traditional C-based solvers, LKH and Concorde, more accessible to Python users,  
1083 **TSPLKHSolver** and **TSPConcordeSolver** are built upon the TSPSolver framework, providing a  
1084 user-friendly interface that allows Python users to effectively utilize the powerful capabilities of LKH  
1085 and Concorde for solving TSP. Here is a simple example solved using the TSPLKHSolver:

```
1086
1087 >>> from ml4tsp import TSPLKHSolver
1088
1089 # 'lkh_max_trials' controls the maximum number of attempts in LKH
1090 >>> lkh_solver = TSPLKHSolver(lkh_max_trials=50000)
1091 >>> lkh_solver.from_txt("data/uniform/test/tsp500.txt")
1092
1093 # Using multi-threading to speed up the solution.
1094 >>> lkh_solver.solve(num_threads=32, show_time=True)
1095 >>> lkh_solver.to_txt("data/uniform/test/tsp500_lkh.txt")
1096
```

### 1097 1098 1099 C.4 EVALUATE ON TSPLIB

1100 We filter problems from the TSPLIB dataset with the number of nodes greater than or equal to 51 and  
1101 less than or equal to 1002, and with EDGE\_WEIGHT\_TYPE as EUC\_2D. We then rescale the node  
1102 coordinates to the range of 0 to 1 globally. To facilitate future research endeavors on TSP, we use  
1103 Concorde to precisely solve these problems and produce the corresponding text files. Furthermore,  
1104 we provide the **TSPLIB4MLDataset** dataset, which can be used to quickly evaluate TSP solvers. In  
1105 the experiments of this paper, we selected problems with the number of nodes ranging from 201 to  
1106 1002 as the test cases, and below is an illustrative evaluation example.

```
1107  
1108 >>> from ml4tsp import TSPLIB4MLEvaluator, ML4TSPGNNSolver
1109  
1110 # Create Evaluator
1111 >>> eval = TSPLIB4MLEvaluator()
1112  
1113 # Create Solver
1114 >>> env = ML4TSPNAREnv(sparse_factor=50)
1115 >>> solver = ML4TSPGNNSolver(
1116     env=env,
1117     encode_device="cuda",
1118     decoder="greedy",
1119     local_search="mcts",
1120     pretrained_path="weights/tsp500_gnn.pt"
1121 )
1122  
1123 # evaluate
1124 >>> eval.evaluate(solver, min_nodes_num=201, max_nodes_num=1002)
1125  
1126     solved_costs  ref_costs    gaps
1127 ts225      10.713846  10.553828  1.516214
1128 tsp225     7.989420   7.895329  1.191729
1129 pr226      5.290722   5.278835  0.225199
1130 gil262    12.054229  12.049518  0.039099
1131 pr264      6.230572   6.200001  0.493082
1132 a280       9.444607   9.238463  2.231368
1133 pr299      6.730816   6.638419  1.391851
1134 lin318    10.410730  10.169940  2.367660
```

rd400	15.408393	15.343968	0.419871
fl417	6.424722	6.285529	2.214497
pr439	9.492026	8.990802	5.574861
pcb442	13.469691	13.364091	0.790177
d493	9.474022	9.350242	1.323819
u574	12.127684	12.022998	0.870709
rat575	13.684484	13.619173	0.479546
p654	7.410115	7.195604	2.981133
d657	12.389867	12.211812	1.458056
u724	14.504233	14.436550	0.468836
rat783	15.308325	15.246543	0.405221
pr1002	16.704860	16.396624	1.879873
AVG	10.763168	10.624413	1.416140

## D SUPPLEMENTARY EXPERIMENTAL RESULTS AND DISCUSSION

### D.1 FULL RECOMPOSITION RESULTS

We show the full experimental results of learning and searching technique recombination for ML4TSP solvers in Table 9. Recombinations that exactly correspond to prior methods are noted in the first column.

### D.2 GENERALIZATION TO VARYING DISTRIBUTIONS

Table 4 shows the generalization results of models trained on TSP-500 to varying distributions, e.g., cluster (gaussian mixture), rotation, explosion etc., instead of uniform Zhou et al. (2023). We find that methods with more complex heuristic search methods and methods with online optimization designs may be less affected by distribution shifts. Meanwhile, different methods have their specialization on different data distributions, yet the ranking may not differ much due to their inherent powerfulness.

Table 14: Generalization results of models trained on TSP-500 to varying distributions, e.g., cluster (gaussian mixture), rotation, explosion etc., instead of uniform. The TSP data of different distributions are from Zhou et al. (2023).

Dataset	Functionality	Training Objective	Learning Search	Construction	Impr. Search	Tour Length	Drop	Time
TSP300-Cluster.3.10	Edge Prediction	SL + Node Norm	-	Greedy	MCTS	9.562	1.482%	0.209s
	Edge Pred	SL + Node Norm	-	Random (n=10)	MCTS	9.493	0.732%	2.016s
	Generation	Generative + Symmetry	-	Greedy	Two-Opt	9.569	1.560%	0.617s
	Generation	Generative + Symmetry	Gradient Search	8 × Greedy	Two-Opt	9.482	0.629%	10.563s
TSP500-Explosion	Edge Pred	SL + Node Norm	-	Greedy	MCTS	11.911	1.298%	1.245s
	Edge Pred	SL + Node Norm	-	Random (n=10)	MCTS	11.817	0.496%	11.617s
	Generation	Generative + Symmetry	-	Greedy	Two-Opt	11.973	1.815%	0.867s
	Generation	Generative + Symmetry	Gradient Search	8 × Greedy	Two-Opt	11.853	0.807%	18.021s
TSP500-Rotation	Edge Pred	SL + Node Norm	-	Greedy	MCTS	12.404	0.745%	1.220s
	Edge Pred	SL + Node Norm	-	Random (n=10)	MCTS	12.357	0.352%	11.063s
	Generation	SL + Symmetry	-	Greedy	Two-Opt	12.472	1.295%	0.852s
	Generation	SL + Symmetry	Gradient Search	8 × Greedy	Two-Opt	12.386	0.592%	17.844s

### D.3 SUPPLEMENTARY RESULTS FOR FIG. 2

Fig. 3 serves as a supplementary figure to Fig. 2, providing the scatter plots for the correlation between solving performance and the learning loss across reference proximity objectives on TSP-50 test sets.

### D.4 SUPPLEMENTARY RESULTS OF RUNTIME-DROP CURVE.

Fig. 4 shows the progress of solving within the heuristic search, showing the variation of the drop with respect to search time in the subsequent heuristic search conducted on predicted heatmaps.

1188  
1189  
1190  
1191  
1192  
1193  
1194  
1195  
1196  
1197  
1198  
1199  
1200  
1201  
1202  
1203  
1204  
1205  
1206  
1207  
1208  
1209  
1210  
1211  
1212  
1213  
1214  
1215  
1216  
1217  
1218  
1219  
1220  
1221  
1222  
1223  
1224  
1225  
1226  
1227  
1228  
1229  
1230  
1231  
1232  
1233  
1234  
1235  
1236  
1237  
1238  
1239  
1240  
1241

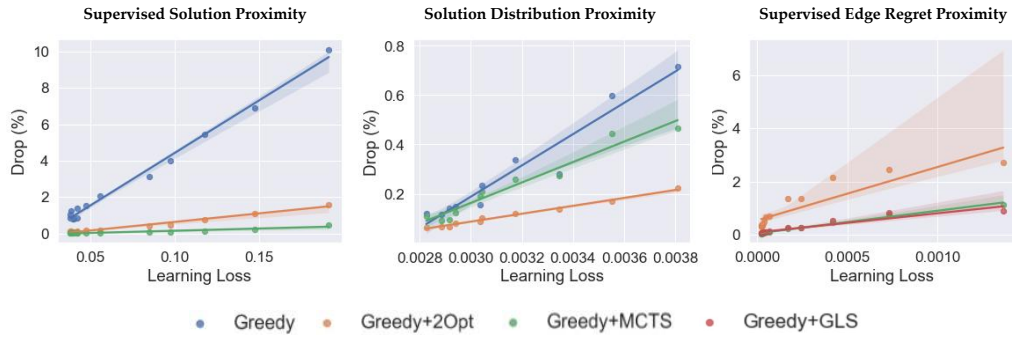


Figure 3: Correlation of performance and learning loss across three reference proximity objectives on TSP50.

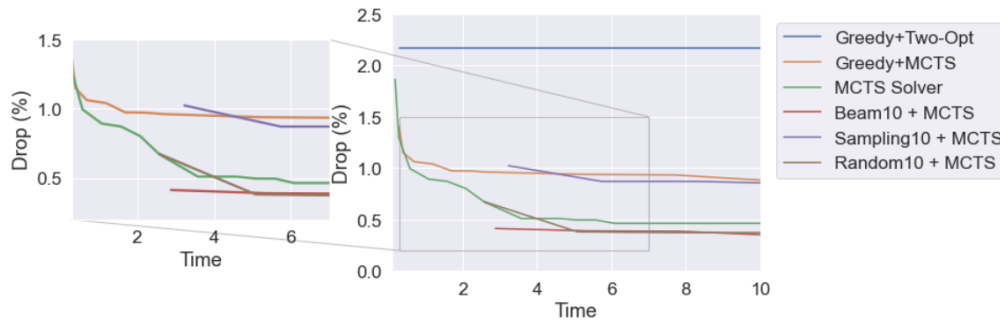


Figure 4: Correlation of performance and runtime.

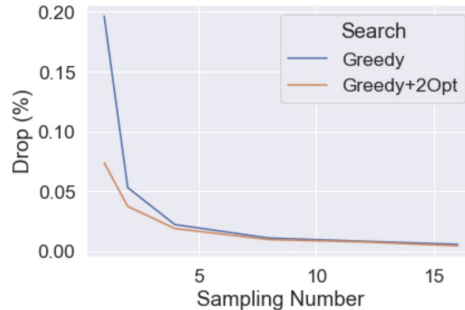


Figure 5: Correlation of performance and sampling number within the estimated distribution for the distribution proximity objective.

#### D.5 SUPPLEMENTARY RESULTS FOR SEC. 4.3.4

To further illustrate the positive impact of prediction diversity on the solving performance, based on the solution distribution proximity objective, Fig. 5 shows the effect of increasing the number of sampling in the estimated solution distribution during solving. As can be observed, with the diversity in neural predictions, the solving performance can be improved through a larger sampling number.

#### D.6 DISCUSSION OF UNSUPERVISED OBJECTIVES

In edge prediction learning functionality, although unsupervised loss provides seemingly reliable training objectives, we observe that the effectiveness of these methods, including both unsupervised solving objective and reinforcement solving objective, relies heavily on heuristic search. Their performance often suffers when subjected to naive construction methods like greedy decoding, with typical drops exceeding 10%. While reproducing these methods, we note that their original implementations heavily relied on the MCTS solver in the search process, where their primary impact

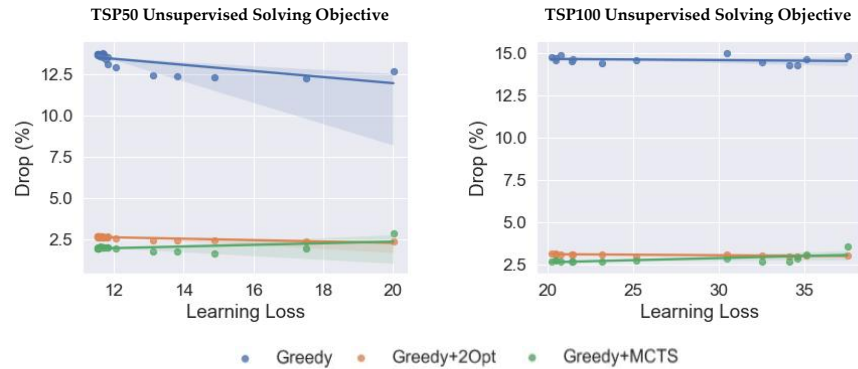


Figure 6: Correlation of performance and learning loss on the unsupervised solving objective.

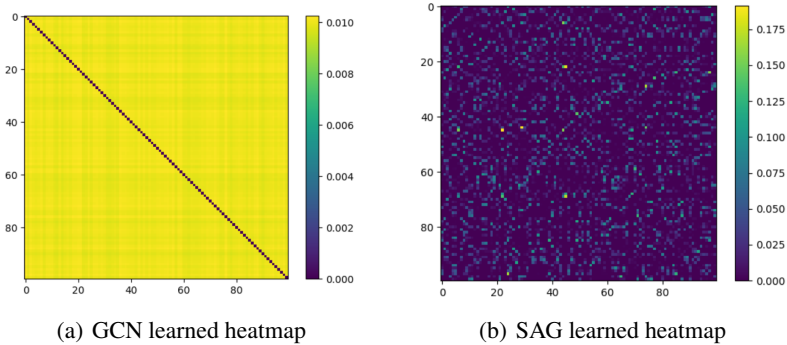


Figure 7: Edge heatmap prediction learned by different graph networks.

lies in providing overall guidance to MCTS. Therefore, incorporating alternative methods during the construction phase to introduce more diversity tends to yield better results. We observe that these methods perform better with Random\_MCTS and Beam\_MCTS. In particular, we verify that the unsupervised solving objective relies on the Scattering Attention GNN (SAG) (Min et al., 2023) to take effect. Fig. 7 shows the effectiveness of SAG in producing sharper heatmaps, avoiding the over-smooth issue as observed in GCN. However, this SAG-learned heatmap still merely brings a greedy solving performance gain from 20% to 13%. Furthermore, we conducted an in-depth analysis of the correlation between solving performance and learning loss within the framework of unsupervised training, as depicted in Fig. 6. However, it’s disappointed to find that a decrease in learning loss did not result in an improvement in solving performance. Thus, it is crucial for edge prediction based unsupervised designs to develop more compatible heuristic search and pursue better integration.

#### D.7 DISCUSSION OF SUPERVISION QUALITY

We observe that the default setting of LKH3 (Helsgaun, 2017) does not generally produce the optimal solutions as claimed by previous works (Qiu et al., 2022; Sun & Yang, 2023). We experiment by adjusting the *max\_trials* hyperparameter in LKH. We gradually increase it and observe that, for TSP-500, the solution quality continues to improve even as we increase the number of trials from 10,000 to 50,000. In this paper, we utilize LKH3 as our source for supervised signals. We employ 500, 5000, and 50000 trials for TSP-50, TSP-100, and TSP-500, respectively.

#### D.8 DISCUSSION OF MCTS

We make an intriguing observation investigating MCTS that the tour length before and after applying MCTS does not show a straightforward proportional relationship. This observation serves as the



1296  
 1297  
 1298  
 1299  
 1300  
 1301  
 1302  
 1303  
 1304  
 1305  
 1306  
 1307  
 1308  
 1309  
 1310  
 1311  
 1312  
 1313  
 1314  
 1315  
 1316  
 1317  
 1318  
 1319  
 1320  
 1321  
 1322  
 1323  
 1324  
 1325  
 1326  
 1327  
 1328  
 1329  
 1330  
 1331  
 1332  
 1333  
 1334  
 1335  
 1336  
 1337  
 1338  
 1339  
 1340  
 1341  
 1342  
 1343  
 1344  
 1345  
 1346  
 1347  
 1348  
 1349

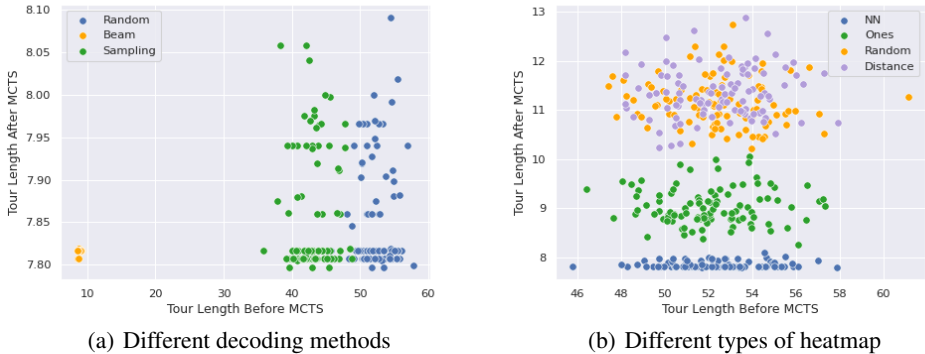


Figure 8: Effects of different decoding methods and heatmap types on MCTS

motivation for us to investigate and develop a range of search methods rooted in MCTS, each incorporating distinct decoding strategies: *Random MCTS*, *Beam MCTS*, and *Sampling MCTS*.

Fig. 8 (a) illustrates the variation in tour length before and after applying these different search methods. The experiments are conducted on the same TSP-100 instance utilizing the same heatmap generated by the model trained with solution proximity objective with node-wise normalization. Each method is sampled 100 times. Note *Beam MCTS*, employing beam search as the sampling strategy, achieves notably shorter average tour lengths before the heuristic search compared to the other two strategies. However, its performance after applying MCTS is found to be comparatively inferior to the other two strategies, as we consistently select the best result obtained from all the samples for each method. This finding aligns with the results presented in Table 9, where, with a sampling number of 50, *Beam MCTS* exhibits an average drop of 0.013%, while the other two methods show a drop of 0.003%, 0.002% respectively.

Furthermore, we investigate the impact of the predicted heatmaps on MCTS. Four types of heatmaps are examined: heatmaps generated by neural networks (NN), all-one heatmaps (Ones), random heatmaps (Random), and distance heatmaps (Distance). Fig. 8 (b) illustrates that the heatmap obtained from the neural network achieved the highest performance compared to the other types. This finding further confirms the significant role of machine learning in enhancing the MCTS method to solve TSP problems.

## E SUPPLEMENTARY DETAILS OF INCORPORATED METHODS

### E.1 TRAINING OBJECTIVES

**Supervised Solution Proximity.** In implementation, we adopt GCN for edge prediction, which receives the node coordinates as the input features and the output edge features would be further mapped by an MLP to predict the probability of including this edge in the optimal solution. The weights of the weighted binary cross-entropy loss are given as  $w_0 = \frac{n^2}{(n^2-2n) \times c}$  and  $w_1 = \frac{n^2}{(2n) \times c}$  where  $c = 2$  denotes the number of classes.

**Supervised Edge Regret Proximity.** Using the same GCN+MLP network architecture, the model is trained with mean squared error loss to predict the regret associated with each edge. Due to the high computational complexity, obtaining the optimal solutions for calculating the corresponding regret is not tractable. Therefore, supervision signals are obtained through LKH3 (Helsgaun, 2017). The max\_trials parameters for TSP-50 and 100 are set as 10 and 5, respectively. In this process, a global reference solution is computed, and the supervision for approximate regret is derived by fixing a particular edge and assessing the degradation in the reference solution caused by fixing that edge.

**Solution Distribution Proximity.** In this paper, we mainly implement the discrete diffusion models (Sun & Yang, 2023; Li et al., 2023) as the representative of generative model based solvers. Taking discrete diffusion models (Sun & Yang, 2023; Li et al., 2023) as representation in this pa-

per, which generates solutions  $\mathbf{S}_0 \in \{0, 1\}^{n \times n}$  by  $T$ -step denoising process from random noises  $\mathbf{S}_T$ , and the latent variables include noised solution  $\mathbf{S}_{1:T}$ . For each entry, the model estimates a Bernoulli distribution indicating whether this entry should be selected. In implementation, each entry of solution is represented by a one-hot vector<sup>3</sup> such that  $\mathbf{S}_0 \in \{0, 1\}^{n \times n \times 2}$ . Following the notations of Ho et al. (2020); Austin et al. (2021), the general framework of diffusion includes a forward noising and a reverse denoising Markov process. The noising process takes the initial solution  $\mathbf{S}_0$  and progressively introduces noise to generate a sequence of latent variables  $\mathbf{S}_{1:T}$ . The denoising process is learned by the model, which starts from the final latent variable  $\mathbf{S}_T$  and denoises  $\mathbf{S}_t$  at each time step to generate the preceding variables  $\mathbf{S}_{t-1}$  based on the instance  $G$ , eventually recovering the target data distribution. The formulation of the denoising process is expressed as  $p_\theta(\mathbf{S}_{0:T}|G) = p(\mathbf{S}_T) \prod_{t=1}^T p_\theta(\mathbf{S}_{t-1}|\mathbf{S}_t, G)$ . The training optimization aims to align  $p_\theta(\mathbf{S}_0|G)$  with the data distribution  $q(\mathbf{S}_0|G)$  using ELBO:

$$\mathcal{L} = \mathbb{E}_q \left[ \sum_{t>1} D_{KL} [q(\mathbf{S}_{t-1}|\mathbf{S}_t, \mathbf{S}_0) \parallel p_\theta(\mathbf{S}_{t-1}|\mathbf{S}_t, G)] - \log p_\theta(\mathbf{S}_0|\mathbf{S}_1, G) \right] + C \quad (7)$$

Specifically, the forward noising process is achieved by multiplying  $\mathbf{S}_t \in [0, 1]^{N \times N \times 2}$  at step  $t$  with a forward transition probability matrix  $\mathbf{Q}_t \in [0, 1]^{2 \times 2}$  where  $[\mathbf{Q}_t]_{i,j}$  indicates the probability of transforming  $E_i$  in each entry to  $E_j$ . We set  $\mathbf{Q}_t = \begin{bmatrix} \beta_t & 1 - \beta_t \\ 1 - \beta_t & \beta_t \end{bmatrix}$  (Austin et al., 2021), where  $\beta_t \in [0, 1]$  such that the transition matrix is doubly stochastic with strictly positive entries, ensuring that the stationary distribution is uniform which is an unbiased prior for sampling. The noising process for each step and the  $t$ -step marginal are formulated as:

$$q(\mathbf{S}_t|\mathbf{S}_{t-1}) = \text{Cat}(\mathbf{S}_t; \mathbf{p} = \mathbf{S}_{t-1}\mathbf{Q}_t) \quad \text{and} \quad q(\mathbf{S}_t|\mathbf{S}_0) = \text{Cat}(\mathbf{S}_t; \mathbf{p} = \mathbf{S}_0\bar{\mathbf{Q}}_t) \quad (8)$$

where  $\text{Cat}(\mathbf{S}; \mathbf{p})$  is a categorical distribution over  $N$  one-hot variables with probabilities given by vector  $\mathbf{p}$  and  $\bar{\mathbf{Q}}_t = \mathbf{Q}_1\mathbf{Q}_2 \cdots \mathbf{Q}_t$ . Through Bayes' theorem, the posterior can be achieved as:

$$q(\mathbf{S}_{t-1}|\mathbf{S}_t, \mathbf{S}_0) = \frac{q(\mathbf{S}_t|\mathbf{S}_{t-1}, \mathbf{S}_0)q(\mathbf{S}_{t-1}|\mathbf{S}_0)}{q(\mathbf{S}_t|\mathbf{S}_0)} = \text{Cat} \left( \mathbf{S}_{t-1}; \mathbf{p} = \frac{\mathbf{S}_t\mathbf{Q}_t^\top \odot \mathbf{S}_0\bar{\mathbf{Q}}_{t-1}}{\mathbf{S}_0\bar{\mathbf{Q}}_t\mathbf{S}_t^\top} \right) \quad (9)$$

The neural network is trained to predict the logits of the distribution  $\tilde{p}_\theta(\tilde{\mathbf{S}}_0|\mathbf{S}_t, G)$ , such that the denoising process can be parameterized through  $q(\mathbf{S}_{t-1}|\mathbf{S}_t, \tilde{\mathbf{S}}_0)$ :

$$p_\theta(\mathbf{S}_{t-1}|\mathbf{S}_t) \propto \sum_{\tilde{\mathbf{S}}_0} q(\mathbf{S}_{t-1}|\mathbf{S}_t, \tilde{\mathbf{S}}_0)\tilde{p}_\theta(\tilde{\mathbf{S}}_0|\mathbf{S}_t, G) \quad (10)$$

**Reinforcement Solving Objective.** For edge prediction functionality, to calculate the gradient estimation by REINFORCE as presented in Eq. 4, we follow Qiu et al. (2022) to build the auxiliary distribution for TSP. Representing the solution as a permutation  $\pi$ , the auxiliary distribution can be formulated as:

$$q_\theta(\pi|G) := \sum_{j=0}^{n-1} \frac{1}{n} \cdot q_\theta(\pi|\pi_0 = j, G) = \sum_{j=0}^{n-1} \frac{1}{n} \cdot \prod_{i=1}^{n-1} q_\theta(\pi_i|\pi_{<i}, G) = \sum_{j=0}^{n-1} \frac{1}{n} \cdot \prod_{i=1}^{n-1} \frac{\exp(\hat{\mathbf{H}}_{\pi_{t-1}, \pi_t})}{\sum_{j=i}^n \exp(\hat{\mathbf{H}}_{\pi_{t-1}, \pi_t})} \quad (11)$$

where  $\hat{\mathbf{H}}$  represents the estimated edge heatmap. With this auxiliary distribution, in each REINFORCE update, we sample 2,000 samples for TSP-50/100 and 120 samples for TSP-500 from  $q_\theta(\pi|G)$  to estimate the gradients.

For the learning functionality of sequential node prediction, instead of establishing the per-step node heatmap from the estimated edge heatmap, sequence models decode each step's node heatmap sequentially. The attention based encoder-decoder model defines a stochastic policy  $p(\pi|G)$  by modeling  $p_\theta(\pi_t|\pi_{t-1}, G)$  at each step. The encoder produces embeddings of all the nodes and the decoder takes the node embeddings, and context of the current state as input, then it uses the attention mechanism to output the attention map over the nodes. With visited nodes masked, the attention map over other unvisited nodes serves as the per-step node heatmap. The gradients are estimated by Eq. 4, where the auxiliary distribution is established upon node heatmaps.

<sup>3</sup>Each entry with  $[0, 1]$  indicates that it is included in  $\mathbf{S}$  and  $[1, 0]$  indicates the opposite.

The symmetric baseline on top of the sequential node prediction objective optimized with RL is implemented referring to Kim et al. (2022). The training objective leverages the symmetries of CO by incorporating the regularization loss of invariant representation  $\mathcal{L}_{inv}$ , the REINFORCE loss with solution symmetry regularization  $\mathcal{L}_{ss}$ , and the REINFORCE loss with both solution and problem symmetry regularization  $\mathcal{L}_{ps}$ . The final loss is written as  $\mathcal{L}_{total} = \mathcal{L}_{ps} + \alpha\mathcal{L}_{inv} + \beta\mathcal{L}_{ss}$ .  $\mathcal{L}_{ss}$  regularizes the symmetric solutions to have the same objective values:

$$\begin{aligned} \mathcal{L}_{ss} &= -\mathbb{E}_{p_\theta(\pi|G)}[R(\pi; G)] \\ \nabla \mathcal{L}_{ss} &\approx -\frac{1}{K} \sum_{k=1}^K \left[ R(\pi^k; G) - \frac{1}{K} \sum_{k=1}^K R(\pi_k; G) \right] \nabla_\theta \log p_\theta \end{aligned} \quad (12)$$

where  $\{\pi^k\}_{k=1}^K$  are the solutions from  $p_\theta(\pi|G)$ .  $\mathcal{L}_{ps}$  regularizes the problem symmetry when two problems have identical optimal solution sets, which is obtained through rotation:

$$\begin{aligned} \mathcal{L}_{ps} &= -\mathbb{E}_{Q^l \sim \mathcal{Q}} \mathbb{E}_{p_\theta(\pi|Q^l(G))}[R(\pi; G)] \\ \nabla \mathcal{L}_{ps} &\approx -\frac{1}{LK} \sum_{l=1}^L \sum_{k=1}^K \left[ R(\pi^{l,k}; G) - \frac{1}{LK} \sum_{l=1}^L \sum_{k=1}^K R(\pi_{l,k}; G) \right] \nabla_\theta \log p_\theta \end{aligned} \quad (13)$$

where  $\mathcal{Q}$  is the distribution of random orthogonal matrices,  $Q^l$  is the  $l^{th}$  sampled rotation matrix, and  $\pi^{l,k}$  is the  $k^{th}$  sample solution of the  $l^{th}$  rotated problem.  $\mathcal{L}_{inv}$  regularizes the model to predict close hidden representations of symmetric problems:

$$\mathcal{L}_{inv} = -S_{cos}(\text{MLP}(h_\theta(G)), \text{MLP}(h_\theta(Q(G)))) \quad (14)$$

where  $S_{cos}$  is the cosine similarity metric,  $h_\theta$  is the neural feature projection,  $Q(G)$  is the rotated problem, and MLP is a projection head.

## E.2 LEARNING-BASED SEARCH

**Gradient Search.** Following T2T (Li et al., 2023), the algorithm starts with an initial solution  $\mathbf{S}_0$  and conducts several iterations to enhance the given solution. Each iteration involves adding a certain degree of noise to disrupt the structure, denoising with objective gradient guidance to obtain a lower-cost solution. The algorithm eventually reports the solution with the lowest objective score. To introduce a controlled degree of disruption to the given solution, we employ  $\mathbf{S}_0 \mathbf{Q}_{\alpha T}$  to derive the distribution of the disrupted solution  $q(\mathbf{S}_{\alpha T} | \mathbf{S}_0)$  as  $N$  Bernoulli distributions, where  $\alpha$  serves as a hyperparameter to control the degree of noise. Subsequently, the disrupted solution  $\mathbf{S}_{\alpha T}$  can be sampled from  $q(\mathbf{S}_{\alpha T} | \mathbf{S}_0)$ . From  $\mathbf{S}_{\alpha T}$ , we employ  $p_\theta(\mathbf{S}_{t-1} | \mathbf{S}_t, G, y^*)$  to perform denoising, which aimed at recovering a potentially lower-cost  $\mathbf{S}'_t$ .

## E.3 LOCAL SEARCH

**Two-Opt.** For a TSP tour sequence  $x_1, \dots, x_p, x_{p+1}, \dots, x_q, x_{q+1}, \dots$ , suppose we select two nodes  $x_p$  and  $x_q$ , and perform a Two-Opt operation by swapping the subsequence between them, the resulting path becomes  $x_1, \dots, x_p, x_q, x_{q-1}, \dots, x_{p+1}, x_{q+1}$ . The difference between the path lengths before and after the swap is denoted as  $reward = D_{p,p+1} + D_{q,q+1} - D_{p,q} - D_{p+1,q+1}$ , where  $D_{i,j}$  represents the distance between node  $i$  and node  $j$ . In each iteration, the two nodes that can obtain the maximum  $reward$  are selected to perform the Two-Opt operation. The iteration terminates when either no more improvements or the maximum number of iterations has been reached. In the experiments of this paper, the maximum number of iterations was set to 5,000.

**Monte Carlo Tree Search.** In our MCTS implementation, we adopt the framework of the MCTS Solver (Fu et al., 2021) while refining certain design aspects.

The first improvement is the Two-Opt module. The MCTS Solver’s Two-Opt strategy involves performing the swap immediately upon identifying a pair of nodes that can yield a gain. In contrast, our approach aligns with the raw Two-Opt implementation, where we select the optimal pair of nodes in each iteration.

The second aspect pertains to our observation that the MCTS derived from the MCTS Solver underutilizes the allocated time slice. When a better solution cannot be found with the current random

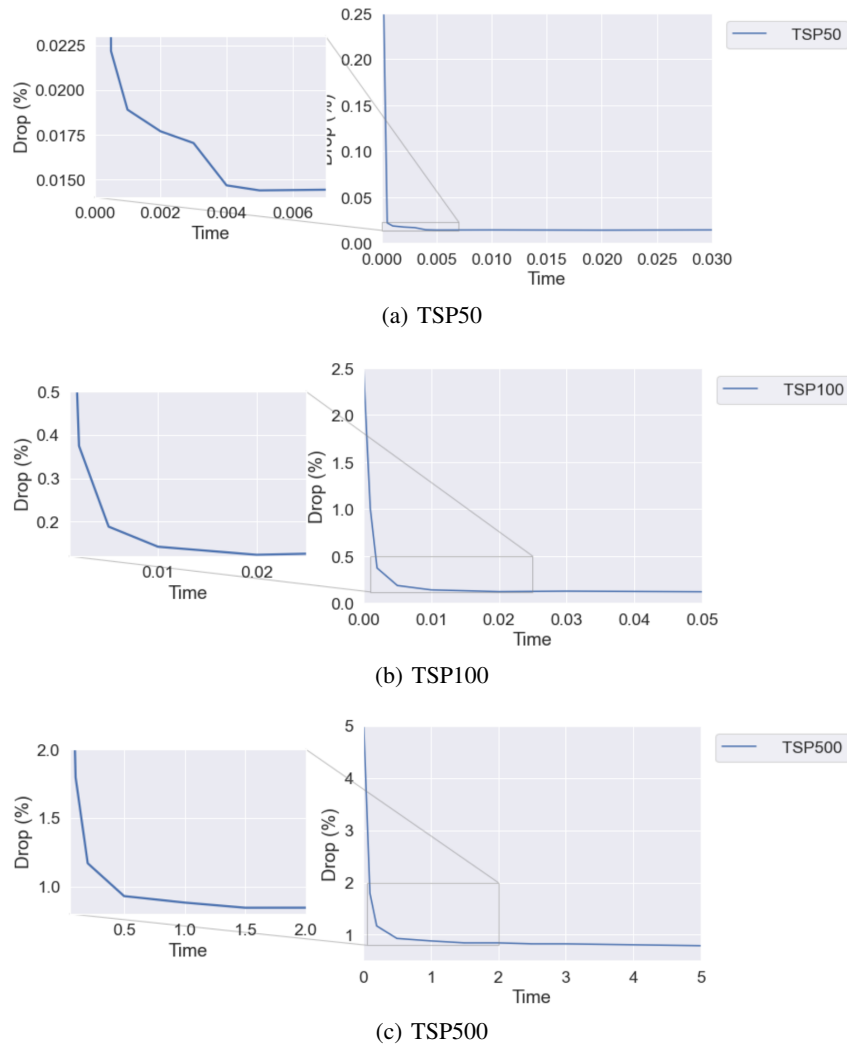


Figure 9: The relationship between the solution quality and the search time of MCTS for different problem scales.

seed, the search terminates prematurely. Additionally, we discover that continuously replacing the random seed somewhat guides the search toward improved solutions, especially on large-scale problems like TSP500, where the gap of the model, which trains with solution proximity objective with node-wise normalization, is reduced from 0.900% to 0.578%.

Based on observation and improvement, we study the optimal search time for MCTS under different problem scales. We take the heatmap encoded by the GNN model and the tour obtained by greedy decoding of this heatmap as a baseline for this investigation. The results are presented in Fig. 9. Based on the results, we set the time limits for the MCTS on problems with 50, 100, and 500 nodes as 0.005, 0.020, and 1.000 seconds, respectively.

Note that although continuous search offers benefits for small-scale problems, the gains are marginal when weighed against the extra time spent. Therefore, to improve the solving speed, we retain the original fixed random number scheme for the TSP50 and TSP100. However, for the TSP500 problem, we implement the optimized scheme to enhance efficiency.

## F NETWORK ARCHITECTURE DETAILS

The network backbones include GNN variants like Graph Convolutional Networks (GCN) (Kipf & Welling, 2016; Joshi et al., 2019), Graph Attention Networks (GAT) (Veličković et al., 2017; Kool et al., 2018), and Scattering Attention GNN (SAG) (Min et al., 2023). In the implementation of non-autoregressive methods, we employ GCN as the model backbone, while for autoregressive methods, we use the transformer (Kool et al., 2018) architecture to build the sequence model, with GAT serving as the essential network backbone. We ensure consistency in GCN and GAT implementations, including the number of layers and feature dimensions. In particular, for the unsupervised solving objectives for edge prediction, due to their reliance on the signal filtering capability of the SAG network, we utilize the SAG network in the implementation of this method, while again keeping its number of layers and feature dimensions consistent.

### F.1 GRAPH CONVOLUTIONAL NETWORKS

**Input Embedding Layer.** Given node vector  $x \in \mathbb{R}^{N \times 2}$  and weighted edge vector  $e \in \mathbb{R}^E$ , we compute the sinusoidal features of each input element respectively. The denoising timestep  $t$  is optional, and it is required when using the diffusion model. Here,  $N$  denotes the number of nodes in the graph, and  $E$  denotes the number of edges,  $t \in \tau_1, \dots, \tau_M$ .

$$\tilde{x}_i = \text{concat}(\tilde{x}_{i,0}, \tilde{x}_{i,1}) \quad (15)$$

$$\tilde{x}_{i,j} = \text{concat} \left( \sin \frac{x_{i,j}}{T^{\frac{d}{2}}}, \cos \frac{x_{i,j}}{T^{\frac{d}{2}}}, \sin \frac{x_{i,j}}{T^{\frac{d}{2}}}, \cos \frac{x_{i,j}}{T^{\frac{d}{2}}}, \dots, \sin \frac{x_{i,j}}{T^{\frac{d}{2}}}, \cos \frac{x_{i,j}}{T^{\frac{d}{2}}} \right) \quad (16)$$

$$\tilde{e}_i = \text{concat} \left( \sin \frac{e_i}{T^{\frac{d}{2}}}, \cos \frac{e_i}{T^{\frac{d}{2}}}, \sin \frac{e_i}{T^{\frac{d}{2}}}, \cos \frac{e_i}{T^{\frac{d}{2}}}, \dots, \sin \frac{e_i}{T^{\frac{d}{2}}}, \cos \frac{e_i}{T^{\frac{d}{2}}} \right) \quad (17)$$

$$\tilde{t} = \text{concat} \left( \sin \frac{t}{T^{\frac{d}{2}}}, \cos \frac{t}{T^{\frac{d}{2}}}, \sin \frac{t}{T^{\frac{d}{2}}}, \cos \frac{t}{T^{\frac{d}{2}}}, \dots, \sin \frac{t}{T^{\frac{d}{2}}}, \cos \frac{t}{T^{\frac{d}{2}}} \right) \quad (18)$$

where  $d$  is the embedding dimension,  $T$  is a large number (usually selected as 10000),  $\text{concat}(\cdot)$  denotes concatenation.

Next, we compute the input features of the graph convolution layer:

$$x_i^0 = W_1^0 \tilde{x}_i \quad (19)$$

$$e_i^0 = W_2^0 \tilde{e}_i \quad (20)$$

$$t^0 = W_4^0 (\text{ReLU}(W_3^0 \tilde{t})) \quad (21)$$

where  $t^0 \in \mathbb{R}^{d_t}$ ,  $d_t$  is the time feature embedding dimension. Specifically, for TSP, the embedding input edge vector  $e$  is a weighted adjacency matrix, which represents the distance between different nodes, and  $e^0$  is computed as above.

**Graph Convolution Layer.** Following Joshi et al. (2019), the cross-layer convolution operation is formulated as:

$$x_i^{l+1} = x_i^l + \text{ReLU}(\text{BN}(W_1^l x_i^l + \sum_{j \sim i} \eta_{ij}^l \odot W_2^l x_j^l)) \quad (22)$$

$$e_{ij}^{l+1} = e_{ij}^l + \text{ReLU}(\text{BN}(W_3^l e_{ij}^l + W_4^l x_i^l + W_5^l x_j^l)) \quad (23)$$

$$\eta_{ij}^l = \frac{\sigma(e_{ij}^l)}{\sum_{j' \sim i} \sigma(e_{ij'}^l)} + \epsilon \quad (24)$$

where  $x_i^l$  and  $e_{ij}^l$  denote the node feature vector and edge feature vector at layer  $l$ ,  $W_1, \dots, W_5 \in \mathbb{R}^{h \times h}$  denote the model weights,  $\eta_{ij}^l$  denotes the dense attention map. The convolution operation integrates the edge feature to accommodate the significance of edges in routing problems.

For TSP, we aggregate the timestep feature with the edge convolutional feature and reformulate the update for edge features as follows:

$$e_{ij}^{l+1} = e_{ij}^l + \text{ReLU}(\text{BN}(W_3^l e_{ij}^l + W_4^l x_i^l + W_5^l x_j^l)) + W_6^l (\text{ReLU}(t^0)) \quad (25)$$

1566 **Output Layer.** The prediction of the edge heatmap in TSP is as follows:

$$1567 \quad e_{i,j} = \text{Softmax}(\text{norm}(\text{ReLU}(W_e e_{i,j}^L))) \quad (26)$$

1568 where  $L$  is the number of GCN layers and  $\text{norm}$  is layer normalization.  
1570

## 1571 F.2 GRAPH ATTENTION NETWORKS

1572 **Input Embedding Layer.** Given node vector  $x \in \mathbb{R}^{N \times 2}$ , we compute initial  $d_h$ -dimensional node  
1573 embeddings  $h_i^{(0)}$  through a learned linear projection with parameters  $W^x$  and  $b^x$ :  $h_i^{(0)} = W^x x_i + b^x$

1574 **Attention Layer.** Following Veličković et al. (2017); Kool et al. (2018), we denote with  $h_1^{(l)}$  the node  
1575 embeddings produced by layer  $l \in \{1, \dots, N\}$  and the attention layer operation is formulated as:

$$1576 \quad \hat{h}_i = \text{BN}^l(h_i^{(l-1)} + \text{MHA}_i^l(h_1^{(l-1)}, \dots, h_n^{(l-1)})) \quad (27)$$

$$1577 \quad h_i^{(l)} = \text{BN}^l(\hat{h}_i + \text{FF}^l \hat{h}_i) \quad (28)$$

1578 where BN represents batch normalization, MHA denotes the multi-head attention layer, and FF refers  
1579 to the node-wise fully connected feed-forward layer.

## 1580 F.3 SCATTERING ATTENTION GNN

1581 **Input Embedding Layer.** Given node vector  $x \in \mathbb{R}^{N \times 2}$ , we compute initial  $d_h$ -dimensional node  
1582 embeddings  $H^0$  through a learned linear projection with parameters  $W^x$  and  $b^x$ :  $H^0 = W^x x_i + b^x$

1583 **Diffusion Module.** Following Min et al. (2023), the diffusion module consists of a cascade of  
1584  $K \in \mathbb{N}$  aggregation (or diffusion) layers with operations that are chosen for each node via an attention  
1585 mechanism. In each layer  $l$ , every node has access to node representations from a set of filters  $\mathcal{F}$  that  
1586 contains a selection of low-pass and band-pass filters as follows:

$$1587 \quad f_{low,r}(H^{l-1}) = A^r H^{l-1} \quad (29)$$

$$1588 \quad f_{band,k}(H^{l-1}) = \Psi_k H^{l-1} \quad (30)$$

1589 where  $\Psi_k \in \mathbb{R}^{n \times n}$  represents a wavelet (Wenkel et al., 2022) at scale  $2^k$ .

1590 To assess the relevance of filter  $f$  to node  $v$ , data-driven scores  $s_f(v)$  are computed. The variable  $H_f^l$   
1591 represents the outcome of applying filter  $f$  to  $H^{l-1}$ . These scores are determined using an attention  
1592 mechanism, which can be defined as:

$$1593 \quad s_f^l := \sigma(H_f^l || H^{l-1}) \mathbf{a}^l \quad (31)$$

1594 where  $||$  denotes the concatenation operation and  $\mathbf{a}^l \in \mathbb{R}^{2d_h}$  denotes the attention vector.

1595 Moreover, the scores are normalized across the filters using the softmax function, denoted as  $\alpha_f(v) =$   
1596  $\text{Softmax}_{\mathcal{F}}(s_f(v))$ . These normalized scores are stored in  $\alpha_f^l$ . Next, the node representations are  
1597 updated through the following process:

$$1598 \quad H_{agg}^l := \sum_{f \in \mathcal{F}} \alpha_f^l \odot H_f^l \quad (32)$$

1599 where  $\odot$  is the element-wise multiplication (applied separately to each column of  $H_f^l$ )

1600 **Output Layer.** The formulas for the output layer is as follows:

$$1601 \quad T = \text{Softmax}(m^l(H_{agg}^l)) \quad (33)$$

1602 where  $m^l$  is the MLP:  $\mathbb{R}^{d_h} \rightarrow \mathbb{R}^{d_h}$ , where  $m^l$  is the MLP:  $\mathbb{R}^{d_h} \rightarrow \mathbb{R}^{d_h}$ . For the TSP problem,  $T$   
1603 represents the assignment matrix in the output, and subsequently, the edge heatmap will be obtained  
1604 by  $TVT^T$ .

Table 15: Design choices of existing major methods.

Method	Offline Learning		Offline Solving		Paradigm
	Learning Functionality	Training Objective	Learning-based Search	Heuristic Search	
GCN (Joshi et al., 2019)	Edge Prediction	Supervised Solution Proximity	None	Greedy / Beam Search	b) c)
Att-GCN (Fu et al., 2021)	Edge Prediction	Supervised Solution Proximity	None	MCTS	c)
DIMES (Qiu et al., 2022)	Edge Prediction	(Meta) Reinforcement Solving Objective	Active Search	Greedy / Sampling / MCTS	b) c)
UTSP (Min et al., 2023)	Edge Prediction	Unsupervised Solving Objective	None	Best-first Local Search	c)
GNNGLS (Hudson et al., 2021)	Edge Regret Prediction	Supervised Edge Regret Proximity	None	Guided Local Search	c)
DIFUSCO (Sun & Yang, 2023)	Solution Generation	Solution Distribution Proximity	None	Greedy / Sampling / MCTS	b) c)
T2T (Li et al., 2023)	Solution Generation	Solution Distribution Proximity	Gradient Search	Greedy / Sampling / MCTS	c)
AM (Kool et al., 2018)	Sequential Node Prediction	Reinforcement Solving Objective	None	Greedy / Sampling	b)
POMO (Kwon et al., 2020)	Sequential Node Prediction	Reinforcement Solving Objective	None	Greedy / Sampling	b)
EAS (Hottung et al., 2021b)	Sequential Node Prediction	Reinforcement Solving Objective	Active Search	Greedy	b)
Sym-NCO (Kim et al., 2022)	Sequential Node Prediction	Reinforcement Solving Objective	None	Greedy / Sampling	b)

## G DISCUSSION FOR THE SYNERGY OF TRAINING AND SOLVING FOR CO

Recall that the solving process of traditional CO solvers primarily involves an online solving procedure based on manually designed heuristics, while the introduction of learning techniques has recently brought about a paradigm shift in this field. In this section, we present the general formulation of CO and specifically TSP, as well as three paradigms for how existing CO solvers exploit machine learning, which serves as a design guideline for our modular framework.

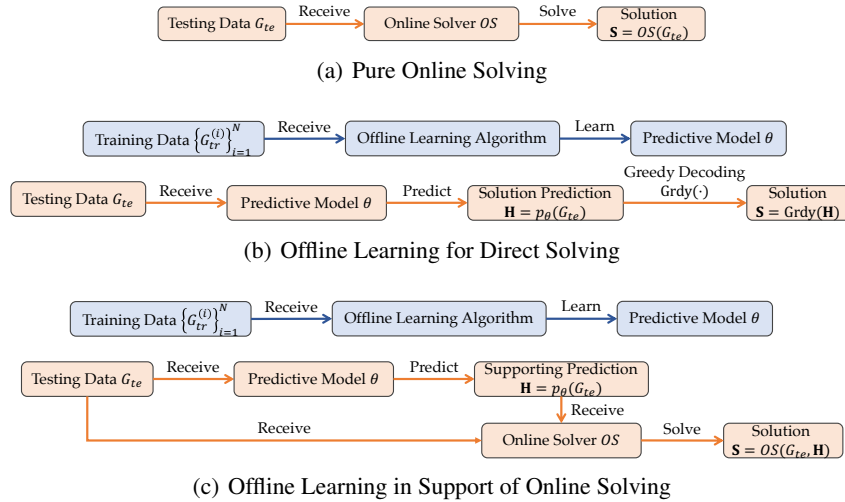


Figure 10: Solving paradigms for existing mainstream CO solvers. Blue and orange stand for offline and online processes, respectively.

**Pure Online Solving.** This paradigm, as shown in Fig. 10 (a), typically comprises classic exact (Applegate et al., 2006) and heuristic (Lin & Kernighan, 1973; Helsgaun, 2017; Fu et al., 2021; Silver et al., 2016) solvers, which operate in a real-time manner without any prior offline learning phase. These solvers rely solely on the data received on the fly according to some unknown distribution and do not leverage any pre-learned knowledge or historical data. They make immediate decisions based on the features of the current problem instance and the objective is to minimize the objective cost for every encountered instance. This classic paradigm has been well-optimized and verified by the operation research community.

However, instances in real-world applications are often from a specific distribution with similar patterns and characteristics (Bengio et al., 2021), e.g., the scheduling of daily deliveries within a particular region may exhibit commonalities. Since this paradigm learns nothing from the pre-existing data, the computation for each instance can be inefficiently repetitive when the data exhibits structural similarity.

**Offline Learning for Direct Solving.** In this paradigm as shown in Fig. 10 (b), the neural solver undergoes an offline learning phase where it learns from historical data before engaging in online solving. The offline learning algorithms produce predictive models that can directly predict solutions based on the given instance features. The primary goal is to learn the predictive models that produce

solution predictions with the minimized average estimation error (for supervised learning) or average objective cost (for unsupervised learning) compared to the optimal solutions.

However, following the classic machine learning mechanism, the neural network is optimized by minimizing the average objective score across the distribution of historical problem instances, diverging from the core target of CO of seeking optimal solutions for every newly encountered instance (Li et al., 2023; Wang & Li, 2022). Without a particular procedure of online search for the specific instance, the predictive model struggles to adapt quality solutions to newly encountered instances, and the typical local minima convergence limits further active search.

**Offline Learning in Support of Online Solving.** This paradigm, as shown in Fig. 10 (c), incorporates an offline learning phase that complements the online solving process. During the offline phase, the solver gathers insights from historical data, which are then leveraged to bolster and optimize the efficiency of the online problem-solving procedures. The offline learning phase can provide valuable support to the online solver through various means, including solution initialization for online solving e.g. naive network prediction (Joshi et al., 2019; Fu et al., 2021), solution distribution estimation e.g. generative modeling (Sun & Yang, 2023; Li et al., 2023), and clues to searching for higher quality solutions e.g. regret estimation for local search (Hudson et al., 2021).

**Overview.** In general, offline learning as a data-driven process can serve as a complement to the per-instance online solving process, such that the solver can excel in both efficiency in processing instances with similar structure and generalizing to every newly encountered instance with sufficient specialized search. Table 15 summarizes the current mainstream algorithms for the TSP problem and categorizes them into the above paradigms to facilitate the follow-up detailed analysis.

## H EXPERIMENTAL DETAILS

All the experiments are performed on GPUs of NVIDIA RTX3090 and a CPU of AMD Ryzen Threadripper 3970X 32-Core Processor. All the test evaluations are performed on a single GPU.

### H.1 IMPLEMENTATION AND HYPERPARAMETERS

Graph convolutional networks:

- **Feature dimensions:** the dimension of the input features for implemented graph networks equals 2 indicating the 2D coordinates of the nodes; the feature dimension of the intermediate layers is set as 256; The output channel dimensions of the networks are set as 2 for TSPGNN, TSPGNNWISE, and TSPDiffusion, and 1 for TSPDIMES, TSPGNN4REG and USTP.
- **Number of layers:** default be set as 12.
- **Sparse factor:** for TSP500, in order to reduce computational and GPU memory requirements, the sparse factor is set as 50, which indicates that each node in the network only considers its nearest 50 nodes for computations. While for TSP50 and TSP100, sparse processing is typically not employed, hence their sparse factor is set as -1.

Graph attention networks:

- **Feature dimensions:** the feature dimension of the intermediate layers is set as 128.
- **Number of layers:** default be set as 3.
- **Number of heads:** the number of heads for the attention is set as 8.

Scattering attention GNN:

- **Feature dimensions:** the feature dimension of the intermediate layers is set as 64.
- **Number of layers:** default be set as 3.

Training objectives:

- **Solution distribution proximity:** We implement the model with 50 inference steps for denoising, and the models are trained with 1000 denoising steps, i.e.,  $T = 1000$ . We



1728 additionally follow Sun & Yang (2023); Li et al. (2023) to apply the technique of denoising  
 1729 diffusion implicit models (DDIMs) (Song et al., 2020) for accelerating inference and solution  
 1730 reconstruction.

- 1731 • **Meta learning objective:** The number of epochs for the inner optimization loop is set as  
 1732 100, and the learning rate is  $5e-2$ . The outer loop can be exactly viewed as the process of  
 1733 active search.
- 1734 • **Unsupervised solving objective:** The weights of the Hamiltonian cycle losses and the no  
 1735 self-loop constraints, i.e.  $\lambda_1$  and  $\lambda_2$  in Eq. 3, are set as 10 and 0.1, respectively.  
 1736

1737 Learning-based search methods:

- 1738
- 1739 • **Gradient Search:** ratio of noise adding in rewrite steps equals 0.4; the number of rewriting  
 1740 steps i.e. guided denoising steps is set as 5 for TSP-50 and 100, and 10 for TSP-500.
- 1741 • **Active Search:** as\_steps is set as 100 and as\_samples is set as 1000.  
 1742

1743 Improved search methods:

- 1744
- 1745 • **Two-opt Search:** The maximum number of iterations is set as 5000.
- 1746 • **Guided LS:** The maximum number of moves is set as 100, and the maximum search time is  
 1747 limited to 10 seconds.
- 1748 • **MCTS:** The maximum search time is one-tenth of the total number of nodes, and the  
 1749 maximum search depth is 10.  
 1750

## 1751 H.2 DETAILS OF EXPERIMENTS

1752  
 1753 **Training Details.** All models are trained with a cosine learning rate schedule starting from  $2 \times 10^{-4}$   
 1754 and ending at 0. For TSP-50, we generally use 1,280,000 random instances for training and train  
 1755 the models for 100 epochs. For TSP-100, we use 1,280,000 random instances and train the models  
 1756 for 50 epochs. We apply curriculum learning and initialize the models from TSP-50 checkpoints.  
 1757 For TSP-500, we use 128,000 random instances and train the models for 50 epochs. We also apply  
 1758 curriculum learning and initialize the models from TSP-100 checkpoints.

1759 **Experimental Details of Fig. 2.** To reflect the correlation between the solving performance and the  
 1760 offline learning quality, we show the scatter plots for the optimality drops with the corresponding  
 1761 learning objective values. During training, we equivalently sample 10 time points for recording and  
 1762 additionally sample the first 5 epochs for their importance as key representatives in the trends. The  
 1763 solid straight lines in the figures represent the fitted trend based on the scatters.

1764 **Experimental Details of Fig. 4.** As the improvement-based search continuously optimizes within  
 1765 the feasible solution space, we can output intermediate solutions at any point to observe the trajectory  
 1766 of solution quality. In our experiments, we set time slots for these improvement-based algorithms  
 1767 to track the variation in solution quality at different running times. Given that 2-opt operates quite  
 1768 swiftly in practice, its descent process is rapid and almost appears as a straight line.  
 1769

## 1770 I LIMITATIONS AND BROADER IMPACTS

1771  
 1772 **Limitations.** The main limitation of this paper lies in the fact that our primary research revolves  
 1773 around ML4TSP and has not yet fully explored all other problems. While we aim to provide insights  
 1774 into the entire ML4CO domain, on the other hand, we intend to thoroughly deconstruct the existing  
 1775 system to explore various aspects of the current major research. Therefore, we have chosen the widely  
 1776 studied and researched TSP problem for comprehensive decomposition and investigation. This also  
 1777 means that the workload of our work solely on ML4TSP is already substantial. We believe that our  
 1778 exhaustive exploration of TSP could also provide valuable insights and reference points for the CO  
 1779 community. Moreover, the framework can be adapted to other CO problems, where the methods  
 1780 requiring reconstruction from scratch are primarily confined to problem-specific heuristic searches.

1781 For the importance of studying ML4TSP and its reference value for other CO problems, we consider  
 TSP as one of the most extensively studied CO problems with the richest learning and searching

1782 techniques, making this analysis representative for ML4CO. Note numerous papers like [Fu et al.](#)  
1783 [\(2021\)](#); [Min et al. \(2023\)](#); [Joshi et al. \(2019\)](#); [Hudson et al. \(2021\)](#); [da Costa et al. \(2020\)](#) concentrate  
1784 on TSP, and it also maintains its own surveys ([Pop et al., 2023](#); [Anbuudayasankar et al., 2014](#);  
1785 [Cheikhrouhou & Khoufi, 2021](#); [Matai et al., 2010](#)) and competitions like AI4TSP ([Zhang et al., 2023](#)),  
1786 highlighting its significant importance. Meanwhile, any other NP problems can reduced to TSP in  
1787 poly-time (since it is NP-hard) to solve, and problems like VRP can directly be broken down to  
1788 TSP ([Luo et al., 2024](#)).

1789 **Broader Impacts.** The proposed principled and comprehensive framework for tackling combi-  
1790 natorial optimization problems can address the lack of unification and offer guidance on crucial  
1791 design principles for ML4TSP and can be generalized to ML4CO. The demonstrated advantages  
1792 of specific techniques, along with the development of new solvers, are expected to inspire further  
1793 research and innovation in the field. The strategic decoupling of existing methods and the unified  
1794 modular framework that reproduces or even enhances the performance of existing methods can  
1795 serve as the codebase and the methodology pool for further research and engineering practices. The  
1796 paper’s insights and observations underscore its potential to enhance the effectiveness of ML-based  
1797 approaches in solving complex optimization problems, ultimately benefiting various application  
1798 domains that rely on combinatorial optimization.

1799  
1800  
1801  
1802  
1803  
1804  
1805  
1806  
1807  
1808  
1809  
1810  
1811  
1812  
1813  
1814  
1815  
1816  
1817  
1818  
1819  
1820  
1821  
1822  
1823  
1824  
1825  
1826  
1827  
1828  
1829  
1830  
1831  
1832  
1833  
1834  
1835